Unitarity of Entanglement and Islands in Two-Sided Janus Black Holes

Dongsu Bak,[a,d] Chanju Kim,[b] Sang-Heon Yi,[a] Junggi Yoon[c]

a) Physics Department, University of Seoul, Seoul 02504 KOREA

b) Department of Physics, Ewha Womans University, Seoul 03760 KOREA

c) School of Physics, Korea Institute for Advanced Study
85 Hoegiro, Dongdaemun-ku, Seoul 02455 KOREA

d) Natural Science Research Institute, University of Seoul, Seoul 02504 KOREA

(dsbak@uos.ac.kr, cjkim@ewha.ac.kr, shyi704@uos.ac.kr, junggiyoon@kias.re.kr)

ABSTRACT

We explore the entanglement evolution of the boundary intervals in the eternal Janus black holes. By the geodesic computation we show that there is a transition of the entanglement characteristic around the Page time, which manifests the unitarity of the evolution. We reproduce and reinterpret these bulk results from the lower dimensional perspectives: one of them is the boundary CFT under the usual AdS/CFT correspondence, while the other one is the one-dimension-lower effective gravity coupled with the radiation background. In this effective theory, we also identify the island of the radiation entanglement wedge and verify the newly proposed quantum extremization method in our model. Our model clarifies that the double holography through a two dimension higher gravity can be incorporated in a concrete and consistent way and that the occurrence of islands is natural in the one-higher dimensional viewpoint.

arXiv:2006.11717v2 [hep-th] 15 Jul 2020

1 Introduction

There have long been riddles on the black hole physics, alluded as the *black hole information paradox*, which was embarked on by the Hawking's semi-classical computation on the black hole background [1, 2]. This issue is initially incurred by the computational results that the black holes behave as thermal objects with the erased information on the in-falling matters forming the black holes. Though there have been numerous attempts to resolve this issue, the complete settlement of the paradox is not yet achieved and the consensus of the status of the problem is not even reached. In fact, the opposite opinions have been made on whether the information could be destroyed or not. See [4–10] for a review.

Even though some physicists [7, 11, 12] argue that gravity or the curved spacetime allows the evolution of the pure state to the mixed one, most of string theorists and AdS/CFT practitioners prefer the preservation of the unitarity of the quantum mechanics. Based on the validity of the AdS/CFT correspondence, the bulk physics is argued to be unitary since it is equivalent to the unitary boundary theory. However, this statement does not provide a clear picture of what happens on the locality assumption on field theory, which is taken as a valid approximation on the near horizon far from the black hole singularity. In other words, the present understanding of the AdS/CFT correspondence does not provide an answer to what is going wrong in the Hawking's results and/or how the bulk locality could be realized in the AdS/CFT context.

From time to time, this information problem reincarnates in disguise. One of the recent reformulation is based on the entanglement characteristic of the Hawking radiation. Roughly speaking, the clash between the unitarity and the semi-classical approximation on the near horizon may be phrased as the seemingly bigamy of the late Hawking radiation with the behind horizon degrees and with the early Hawking radiation, which violates the monogamy property of the entanglement in quantum mechanics. One of the proposed resolution in this problem is to abandon the semi-classical features by introducing high energy curtain (firewall) [14, 15], while another one is to preserve the semi-classical picture but to make a bit bold and clever identification between the behind horizon degrees and the emitting Hawking radiation (ER=EPR) [16]. Though these proposals evade the apparent contradiction, the information loss problem is still far from the understanding. For instance, the Page's curve [17] for the entanglement evolution of the Hawking radiation needs to be explained in an appropriate way.

Very recently, the explicit computation for the entanglement of the Hawking radiation in the Jackiw-Teitelboim model [18, 19] is performed and the entanglement evolution is shown to follow the Page's curve by using the quantum extremal surface (QES) prescrip-

tion [22–24] for the entanglement wedge [20] (See also [21]). In a more recent work [25], the missing ingredient in gravity theory to the entanglement computation is clearly identified and called as the island of the entanglement wedge. In this work, a new extremization prescription for the generalized entropy is proposed by including the islands. Furthermore, the QES is argued to become the ordinary Ryu-Takayangi surface [26, 27] in one more higher dimensional holographic setup.

In this paper, we take a consistent top-down approach to one more higher dimensional holographic model, known as the holographic dual to interface CFT (ICFT) [28]. This model contains solutions known as the Janus black holes [29], which is our main concern in the following. Since this model may be embedded consistently in string/M-theory as a low energy limit, our analysis might be extended into the full string theory level. Interestingly, we do not introduce any 'end of world branes' in our model. Rather, we describe the low dimensional gravity coupled to the thermal radiation from the viewpoint of the effective reduction of the higher dimensional one. Our model provides a different perspective over the bottom-up brane models [31–33] in the sense that the usual holography method could be applied without further machinery.

Our paper is organized as follows. In Section 2, we provide some details on our model and on Janus black hole solutions. Especially, various coordinates in our setup are introduced for later convenience. In Section 3, the entanglement entropy is briefly reviewed and the holographic entanglement entropy (HEE) is computed for RR/LL geodesics. In Section 4, we have computed the HEE for RL geodesics. We have presented the Page curve of our black hole model and the unitarity of the entanglement in Section 5. In this section, we have also commented on the evolution of the mutual information of the Hawking radiation in our setup. In Section 6, we provide the two-dimensional gravity interpretation of our results and reproduce our results from the generalized entropy extremization procedure. In Section 7, we provide another perspective by using ICFT on our results, which is the boundary viewpoint on our model. In Section 8, we provide interesting new aspects to the entanglement island pictures by using our model. In the conclusion, we summarize our results and present some future directions. In Appendices A and B, we provide some details on formulae and the effective CFT$_2$ viewpoint, respectively.

Note added: During finalizing our work, we have encountered the upload of arXiv: 2006.04851 [hep-th] [34], which overlaps with our work in the perspective.

2 Janus black holes in three dimensions

In this section, we shall investigate the holography of thermo-field double (TFD) dynamics of the Janus ICFT$_2$, whose gravity dual is the two-sided version of 3d Janus black hole. It is known that the Janus geometry arises as a classical solution to the system of Einstein gravity coupled to negative cosmological constant with a minimal massless scalar field whose action is given by

$$I_{\text{gravity}} = \frac{1}{16\pi G} \int_{M_{d+1}} d^{d+1}x \left[R - g^{ab}\partial_a\phi\partial_b\phi + \frac{d(d-1)}{\ell^2} \right] . \tag{2.1}$$

The Janus geometry can be found for arbitrary dimensions. For $(d+1) = 3$ and 5, this system can be consistently embedded into the Type IIB supergravity and hence, via the AdS/CFT correspondence, the microscopic understanding of dual ICFT$_d$ system can be obtained [28, 35]. The scalar field here originates from the dilaton field of the underlying Type IIB supergavity and hence it is holographically dual to the CFT$_d$ Lagrangian density. The equations of motion read

$$g^{ab}\nabla_a\nabla_b\phi = 0 \,,$$

$$R_{ab} = -\frac{d}{\ell^2}g_{ab} + \partial_a\phi\partial_b\phi \,. \tag{2.2}$$

The vacuum solution is the AdS$_{d+1}$ space with curvature radius ℓ and an everywhere constant scalar field. The Janus geometry is a nontrivial domain-wall solution in which the scalar field and metric approach those of the vacuum solutions. Below, we shall be specialized in three dimensions for simplicity.

The three-dimensional Janus solution is given by [35]

$$ds^2 = \ell^2 \left[dy^2 + f(y)\, ds^2_{\text{AdS}_2} \right] \,,$$

$$\phi(y) = \frac{1}{\sqrt{2}} \ln \left(\frac{1 + \sqrt{1 - 2\gamma^2} + \sqrt{2}\gamma \tanh y}{1 + \sqrt{1 - 2\gamma^2} - \sqrt{2}\gamma \tanh y} \right) \,, \tag{2.3}$$

where

$$f(y) = \frac{1}{2} \left(1 + \sqrt{1 - 2\gamma^2} \cosh 2y \right) \qquad \text{with} \qquad \gamma < \frac{1}{\sqrt{2}}. \tag{2.4}$$

As $y \to \pm\infty$, the value of the scalar field approaches $\pm\phi_{\text{as}}$ where $\phi_{\text{as}} = \frac{1}{\sqrt{2}}\text{arctanh}\sqrt{2}\gamma$. For our two-sided Janus black hole, we choose the AdS$_2$ part as the global AdS$_2$

$$ds^2_{\text{AdS}_2} = \frac{d\lambda^2 - d\tau^2}{\cos^2\lambda} = dq^2 - \cosh^2 q\, d\tau^2 \,, \qquad \frac{1}{\cos\lambda} = \cosh q \,, \tag{2.5}$$

where $\lambda \in (-\lambda_\infty, \lambda_\infty)$ with λ_∞ ranged over $[0, \frac{\pi}{2})$ and $q \in (-q_\infty, q_\infty)$ with q_∞ over $[0, \infty)$. The R and L boundaries are at $|y| = \infty$ with R/L boundary coordinates $(\tau, +/-\lambda_\infty)$ (See below for the details). One may introduce the coordinate μ defined by

$$d\mu = \frac{dy}{\sqrt{f(y)}} , \tag{2.6}$$

which is ranged over $[-\mu_0, \mu_0]$ with the boundary value $\mu_0 = \int_0^\infty \frac{dy}{\sqrt{f(y)}}$. One can evaluate the integral exactly to

$$\mu_0 = \frac{1}{\kappa_+} \mathbf{K}\left(\frac{\kappa_-^2}{\kappa_+^2}\right) = \frac{\pi}{2}\left(1 + \frac{3}{8}\gamma^2 + \mathcal{O}(\gamma^4)\right) , \tag{2.7}$$

where $\mathbf{K}(x)$ is the first kind of complete elliptic integral and $\kappa_\pm^2 = \frac{1}{2}\left(1 \pm \sqrt{1 - 2\gamma^2}\right)$. In the last equality, we presented its Taylor expansion with respect to the deformation parameter γ. From this, one finds $\mu_0 \geq \frac{\pi}{2}$, which is a consequence of the deformation. In this coordinate system, the metric becomes

$$ds^2 = \ell^2 f(\mu) \left[d\mu^2 + ds_{\text{AdS}_2}^2\right] . \tag{2.8}$$

For the Rindler type solution valid for the right/left wedge, we perform a coordinate transformation

$$w = \frac{\cos\tau}{\cos\lambda}, \qquad \tanh\frac{Lt}{\ell^2} = \frac{\sin\tau}{\sin\lambda} , \tag{2.9}$$

and then the AdS$_2$ metric is replaced by the Rindler metric

$$ds_{\text{AdS}_2}^2 = -\frac{(w^2 - 1)L^2}{\ell^4}dt^2 + \frac{dw^2}{w^2 - 1} . \tag{2.10}$$

This leads to the Rindler-type Janus black hole solution [29] where the horizon is located at $w = 1$ with the horizon size L and $w \in [1, \infty)$ describes the region outside horizon.

Without deformation, $\gamma = 0$, one has the standard planar BTZ black hole [36], given by the geometry

$$ds^2 = \ell^2 \left[dy^2 + \cosh^2 y \, ds_{AdS_2}^2\right] , \tag{2.11}$$

and, by integrating (2.6), one has

$$\cos\mu = \frac{1}{\cosh y} . \tag{2.12}$$

Indeed, through the coordinate transformation

$$\frac{L}{r} = \frac{\cos\mu}{\sqrt{w^2 - \sin^2\mu}} , \qquad \sinh\frac{Lx}{\ell^2} = \frac{\sin\mu}{\sqrt{w^2 - \sin^2\mu}} , \tag{2.13}$$
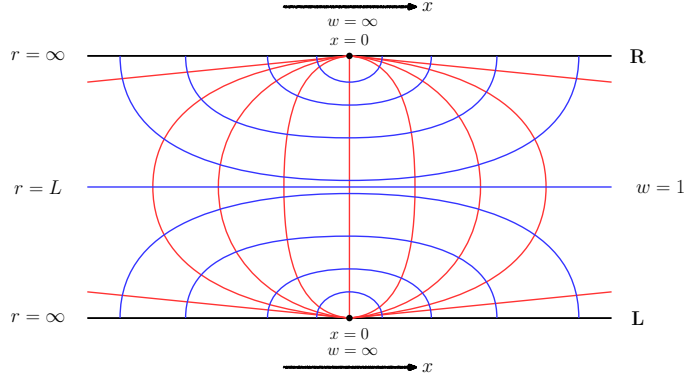
4

Figure 1: We draw the constant t section of the BTZ spacetime where we show (μ, w) together with (r, x) coordinates. The middle line with $w = 1$ and $r = L$ represents the horizon. The red lines are representing constant μ surfaces whereas the blue lines are for constant w surfaces. The top/ bottom line represents the spatial direction of the R/L boundary respectively.

the $\gamma = 0$ geometry is reduced to the conventional form of planar BTZ metric

$$\mathrm{d}s^2 = -\frac{(r^2 - L^2)}{\ell^2}\mathrm{d}t^2 + \frac{\ell^2}{r^2 - L^2}\mathrm{d}r^2 + \frac{r^2}{\ell^2}\mathrm{d}x^2. \tag{2.14}$$

One finds that both coordinates τ and μ are ranged over $[-\frac{\pi}{2}, \frac{\pi}{2}]$ and x can be compactified by $x \sim x + L_s$ as system possesses a translational symmetry in the x directions. With the Janus deformation breaking the translational symmetry, we shall be concerned with the planar Janus black holes where the spatial extent is noncompact by sending the size L_s to infinity.

In Figure 1, we depict the shape of constant t slice of the undeformed BTZ geometry where we show (μ, w) together with (r, x) coordinates. The top/bottom line represents the spatial direction of the R/L boundary spacetime. The R/L boundaries are parametrized either by (t, x) or by $(\tau, \pm\lambda_\infty)$ where the two coordinate systems are related by

$$\tanh\frac{Lx}{\ell^2} = \frac{\epsilon(x)}{w} = \epsilon(x)\frac{\cos\lambda_\infty}{\cos\tau} ,$$
$$\tanh\frac{Lt}{\ell^2} = \pm\frac{\sin\tau}{\sin\lambda_\infty} , \tag{2.15}$$

where $\epsilon(x)$ denotes the sign function of x and $+/-$ does for the R/L boundary spacetime, respectively. These relations may be inverted as

$$\tan\lambda_\infty = \frac{\cosh\frac{Lt}{\ell^2}}{\sinh\frac{L|x|}{\ell^2}}, \qquad \tan\tau = \frac{\sinh\frac{Lt}{\ell^2}}{\cosh\frac{Lx}{\ell^2}} , \tag{2.16}$$

5

which will be useful in the following. The middle line corresponds to the horizon location with $w = 1$ (or $r = L$). The red lines are denoting constant μ trajectory where the μ coordinate runs over $[-\pi/2, \pi/2]$ for the BTZ geometry. The blue curves represent constant w surfaces. A few comments are in order. First is the well-known time translation isometry of the BTZ geometry. This leads to the boundary time translational symmetry $t \to t + dt$ with $t_{R/L} = \pm t$ where $t_{R/L}$ denotes respectively the time coordinate of R/L boundary, both going in the positive direction in our choice. Secondly, the region of $x \to \infty$ merges to a point at the spatial section of the boundary of global AdS_3 geometry and the same is true for the region of $x \to -\infty$. Hence the R and L boundaries form a single boundary that is the boundary of the global AdS_3 spacetime [37]. Nonetheless, the R and L boundary theories are causally disconnected with each other completely.
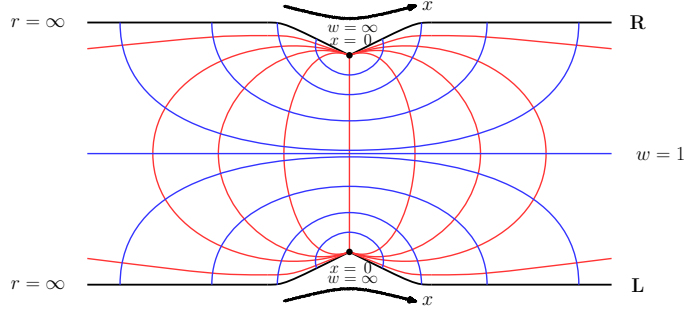

Figure 2: We draw the constant t section of the two-sided Janus black hole where we show (μ, w) together with (r, x) coordinates. The middle line with $w = 1$ represents the horizon. The red lines are representing constant μ surfaces whereas the blue lines are for constant w surfaces. The μ coordinate is ranged over $[-\mu_0, \mu_0]$ with $\mu_0 > \pi/2$. This leads to the $x = 0$ angled-joints of the R-L boundaries.

In Figure 2, we draw also the constant t spatial section of the Janus black hole spacetime. This geometry is asymptotically AdS; one may map its asymptotic region to that of the BTZ spacetime. The coordinates in this region can be identified as

$$
\begin{aligned}
\frac{r}{L} &\simeq \sqrt{(w^2 - 1)f + 1}\,, \\
\sinh \frac{Lx}{\ell^2} &\simeq \epsilon(x) \frac{\sqrt{f - 1}}{\sqrt{(w^2 - 1)f + 1}}\,,
\end{aligned} \tag{2.17}
$$

with t and w coordinates defined by (2.9). The boundary coordinates (t, x) are defined by (2.15) from which the inverse in (2.16) is followed. In Figure 2, the red lines are for

the constant μ surface where μ is ranged over $[-\mu_0, \mu_0]$ with $\mu_0 > \pi/2$ as a result of deformation. This leads to the angled-joints at $x = 0$ of Figure 2 where some interface degrees are located in a certain sense.

The Gibbons-Hawking temperature of the Janus black hole can be identified from the Euclidean version of the solution obtained by Wick rotation $t = -it_E$. By requiring the regularity of this Euclidean geometry at $w = 1$, one finds

$$T = \frac{L}{2\pi\ell^2} \,, \tag{2.18}$$

which agrees with that of the undeformed BTZ black hole. The mass of the system can be obtained by studying the holographic stress-energy tensor leading to [29]

$$E = \frac{c}{6}\pi T^2 L_s \,, \tag{2.19}$$

where $c = \frac{3\ell}{2G}$ is the central charge of the boundary ICFT and we take the system size L_s large enough. For simplicity, we take an interval $x \in [-L_s/2, L_s/2]$ with $x = 0$ the place where the interface is located. Similarly, the Bekenstein-Hawking entropy of the system can be obtained as [29]

$$S = \frac{c}{3}\pi T L_s + S_I \,, \tag{2.20}$$

where the interface contribution

$$S_I = \frac{c}{6}\ln A \,. \tag{2.21}$$

Here, A denotes a bulk parameter defined by

$$A \equiv \frac{1}{\sqrt{1 - 2\gamma^2}} = \cosh\sqrt{2}\phi_{\mathrm{as}} \,. \tag{2.22}$$

This interface entropy is a measure of the interface QM degrees of freedom and the corresponding number of ground states is given by e^{S_I}, whose quantum wave functions are centered at the interface.

Let us now describe the dual field-theory side. The bulk scalar field is dual to an exactly marginal scalar operator $O(x, t)$. The boundary value of the scalar field implies turning on the operator O with a source term: The CFT_2 is deformed by the perturbation $\int d^2x\, g(\epsilon(x)\phi_{\mathrm{as}})O(x, t)$ which breaks x translation invariance explicitly. One has in general $g(z) = z + O(z^2)$, which can be identified to all orders in our AdS/CFT correspondence. This basically leads to an ICFT

$$\mathrm{ICFT} = \mathrm{CFT}_- \times \mathrm{QM}_0 \times \mathrm{CFT}_+ \,, \tag{2.23}$$

where QM_0 denotes the interface QM degrees of freedom. This system preserves the one dimensional conformal symmetries of $SO(1, 2)$. See Figure 3.

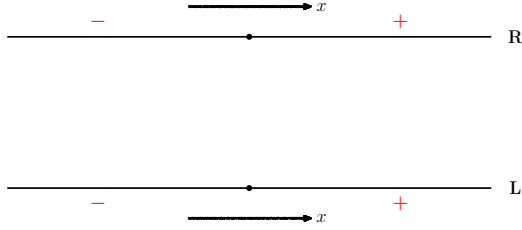Figure 3: We draw ICFT × ICFT living on the L and R boundaries of our two-sided Janus black hole. Each ICFT consists of three components of $CFT_- \times QM_0 \times CFT_+$, which preserves 1d conformal symmetries of $SO(1,2)$.

For our two-sided Janus black hole, one has R and L ICFT theories at the same time ICFT × ICFT, which are initially entangled in a particular manner. Following the Hartle-Hawking construction of wave function [39], one gets a TFD initial state

$$|\psi(0,0)\rangle = \frac{1}{\sqrt{Z}} \sum_n e^{-\frac{\beta}{2}E_n}|n\rangle \otimes |n\rangle\,, \qquad (2.24)$$

where $|n\rangle$ is the energy eigenstate of ICFT Hamiltonian H with the energy eigenvalue E_n. The subsequent Lorentzian time evolution is then given by

$$|\psi(t_{\mathrm{L}}, t_{\mathrm{R}})\rangle = e^{-i(t_L H \otimes I + t_R I \otimes H)}|\psi(0,0)\rangle\,. \qquad (2.25)$$

This gives a desired TFD dynamics of our ICFT, which will serve as our main framework in the field theory side. It is clear that the state with $t_R = -t_L = t$ is t-independent which is consistent with the time-like Killing symmetry of our black hole geometry. In this work we shall be interested in the time evolution with $t_L = t_R = t$ which indeed becomes nontrivial.

Finally let us briefly comment upon the shadow region of interfaces in the bulk. Note, in our Janus black hole system, the x-translational symmetry is broken by the presence of the interfaces and the "entropy density" becomes x-dependent. In our geometrical setup, the entropy is defined on the horizon side and, hence, one needs a map which relates the boundary coordinate x to the horizon coordinate. We use here the boundary horizon map based on null geodesics emanating from the boundary in a hypersurface orthogonal manner, whose details are described in [29]. For a given boundary point x, the horizon

coordinate can be identified as [29]

$$\mu_H = \left(\mu_0 - \frac{\pi}{2}\right)\epsilon(x) + \arctan\sinh\frac{2\pi x}{\beta}. \qquad (2.26)$$

With this boundary horizon map, one finds there is an excluded region specified by $-\mu_I \leq \mu \leq \mu_I$ where μ_I equals to $\mu_0 - \frac{\pi}{2} = \frac{3\pi}{16}\gamma^2 + O(\gamma^4)$. This excluded region may be regarded as an extra bulk space created and affected by the interfaces, which shall be dubbed as the shadow of the interfaces. However, this shadow region is not sharply defined as we shall discuss further below. For our later purpose, we shall choose μ_I (and the corresponding shadow) as

$$\mu_I = \mu_0 - \left[\frac{\pi}{2} + \left(\sqrt{2}\ln(e + \sqrt{e^2 - 1}) - \frac{\pi}{2}\right)\tanh^2(A - 1)\right], \qquad (2.27)$$

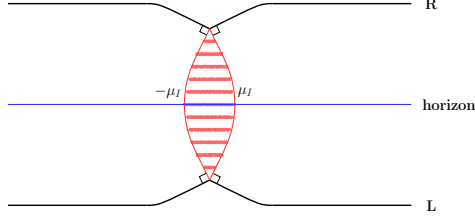instead of $\mu_0 - \frac{\pi}{2}$. We depict this shadow in Figure 4.

Figure 4: We draw the shadow region specified by $\mu = constant$ slices ranged over $\mu \in [-\mu_I, \mu_I]$. One may integrate out the bulk degrees in this shadow region and view that the resulting 2d gravity theories are living on $\mu = \pm\mu_I$ slices, respectively.

One may integrate out the bulk degrees in this shadow to get 2d gravity theories $\mathrm{Grav}_\pm$ defined on $\mu = \pm\mu_I$ slices whose dual quantum mechanical systems may be denoted by $\mathrm{QM}_\pm$ respectively. Therefore, one may alternatively view our ICFT as

$$\mathrm{ICFT} = \mathrm{CFT}_- \times \mathrm{QM}_- \times \mathrm{QM}_+ \times \mathrm{CFT}_+. \qquad (2.28)$$

In this manner, one may get a picture of 2d gravities coupled to 2d CFT's.

3 Entanglement of an interval

3.1 Review: Entanglement Entropy

In this section, we shortly review the entanglement entropy. Let us consider a bi-partite system $\mathcal{H} = \mathcal{H}_A \otimes \mathcal{H}_B$. From the reduced density matrix $\rho_A = \mathrm{tr}_B\rho$ of the subsystem A,

the entanglement entropy of the subsystem A is given by

$$S_{EE} = -\ln\left(\rho_A \ln \rho_A\right). \tag{3.1}$$

In general, it is difficult to evaluate this entanglement entropy because of the logarithm of the density matrix. Instead, we evaluate $\mathrm{tr}\rho_A^n$ and take a limit to get the entanglement entropy.

$$S_{EE} = -\lim_{n\to 1}\frac{\partial}{\partial n}\mathrm{tr}(\rho_A^n). \tag{3.2}$$

The trace of the nth power of the density matrix can be evaluated by n replicas of the original system [30]. The boundary condition of the replica trick for the subsystem A can be incorporated by twist operators $\Phi_n^{\pm}(z)$, and $\mathrm{tr}\rho_A^n$ can be computed by inserting twist operators at the end of the interval A:

$$\mathrm{tr}\rho_A^n = \langle \Phi_n^+(z)\Phi_n^-(w)\rangle = \frac{1}{\left[\frac{\beta}{2\pi\varepsilon}\sinh\left(\frac{\pi L}{\beta}\right)\right]^{2\Delta_n}}, \tag{3.3}$$

where Δ_n is the conformal dimension of the twist operator $\Phi_{\pm}^n$

$$\Delta_n = \frac{c}{12}\left(n - \frac{1}{n}\right). \tag{3.4}$$

For example, the entanglement entropy of an interval of which length is L_0 is found to be

$$S_{EE} = S_\varepsilon + \frac{c}{3}\ln\left[2\sinh\left(\frac{\pi L_0}{\beta}\right)\right], \tag{3.5}$$

where S_ε corresponds to the contribution of the short distance degrees with the cutoff scale ε as

$$S_\varepsilon \equiv \frac{c}{3}\ln\left[\frac{\beta}{4\pi\varepsilon}\right]. \tag{3.6}$$

In a boundary CFT (BCFT) or ICFT, the degree of freedom living on the boundary or the interface give a contribution to the entanglement entropy as

$$S_{EE} = S_\varepsilon + \frac{c}{3}\ln\left[2\sinh\left(\frac{\pi L}{\beta}\right)\right] + \ln g, \tag{3.7}$$

where $\ln g$ is the boundary entropy [38]. In the Janus ICFT, the boundary entropy can be evaluated from the two point function of the twist operators by the conformal perturbation:

$$\langle\Phi_+(z)\Phi_-(w)\rangle_\gamma = \langle\Phi_+(z)\Phi_-(w)\rangle + \gamma\int d^2x\,\epsilon(x^1)\langle\Phi_+(z)\Phi_-(w)\mathcal{O}(x)\rangle + \mathcal{O}(\gamma^2). \tag{3.8}$$

10

The leading contribution of order $\mathcal{O}(\gamma)$ is universal up to OPE coefficient because of the universal form of three point function:

$$\gamma \int d^2x \; \epsilon(x^1)\langle\Phi_+(z)\Phi_-(w)\mathcal{O}(x)\rangle = \gamma \int \frac{d^2x \; \epsilon(x^1)\mathcal{C}_{\Phi_+\Phi_-\mathcal{O}}}{(z-w)^{2\Delta_n-2}(z-x)^2(w-x)^2} \,. \tag{3.9}$$

However, this gives a correction of order $\mathcal{O}(c^0)$ to the conformal dimension and the normalization of the two point function of the twist operators. Hence, in large c limit, the non-zero correction to the entanglement entropy is of order $\mathcal{O}(\gamma^2)$.

$$S_{EE} = S_\varepsilon + \frac{c}{3}\ln\left[2\sinh\left(\frac{\pi L}{\beta}\right)\right] + \mathcal{O}(\gamma^2 c) \,. \tag{3.10}$$

Though the $\mathcal{O}(\gamma^2)$ correction is not universal, one can deduce it from the conformal perturbation of the free energy of the Janus ICFT:

$$\beta F = -\ln Z = \beta\mathcal{F} - \ln g = \beta F_0 + \gamma^2 \beta F_2 + \cdots \,. \tag{3.11}$$

The $\mathcal{O}(\gamma^2)$ correction is found to be [29]

$$\gamma^2 \beta F_2 = \frac{1}{2}\gamma^2 \int d^2x\, d^2y \; \epsilon(x^1)\epsilon(x^1)\langle\mathcal{O}(x)\mathcal{O}(y)\rangle = -\frac{\ell}{4G}\gamma^2 = -\frac{c}{6}\gamma^2 \,, \tag{3.12}$$

and, this leads to

$$\ln g = \frac{c}{6}\gamma^2 + \mathcal{O}(c\gamma^4) \,. \tag{3.13}$$

Therefore, we have

$$S_{EE} = S_\varepsilon + \frac{c}{3}\ln\left[2\sinh\left(\frac{\pi L}{\beta}\right)\right] + \frac{c}{6}\gamma^2 + \mathcal{O}(\gamma^4) \,. \tag{3.14}$$

3.2 Holographic Entanglement Entropy

Now, we will study the entanglement entropy of a single interval $\mathcal{I}$ from the bulk geometry by using the AdS/CFT correspondence. Holographically, the entanglement entropy can be evaluated from the area of the Ryu-Takayanagi surface [26] whose boundary is the interval $\mathcal{I}$

$$S_{EE} = \frac{\text{Area}}{4G} \,. \tag{3.15}$$

In AdS$_3$/CFT$_2$, the area of the Ryu-Takayanagi surface corresponds to the geodesic distance connecting to both ends of the interval $\mathcal{I}$. For this, we consider the metric in (2.8) of the three-dimensional Janus black hole solution [29] with a coordinate transformation $w = \cosh\rho$ in (2.10)

$$ds^2 = \ell^2\left[dy^2 + f(y)\left(-\frac{L^2}{\ell^4}\sinh^2\rho \; dt^2 + d\rho^2\right)\right] \,. \tag{3.16}$$

For simplicity, let us consider a geodesic on the constant time-slice:

$$t = \text{constant} . \tag{3.17}$$

The rest of the geodesic equations are given by

$$f(y)\frac{d\rho}{ds} = \frac{\mathcal{E}}{\ell} \quad , \quad \left(\frac{dy}{ds}\right)^2 + \frac{\mathcal{E}^2}{\ell^2 f(y)} = \frac{1}{\ell^2} , \tag{3.18}$$

where $\mathcal{E}$ is a constant. Let us consider the simplest case:

$$\mathcal{E} = 0 . \tag{3.19}$$

This corresponds to a geodesic with constant t and ρ:

$$t = \text{constant} \quad , \quad \rho = \text{constant} . \tag{3.20}$$

Note that this geodesic is presented as the blue line[1] in Figure 2. Now, one can easily integrate (3.18) to obtain the geodesic distance between two points corresponding to y_∞ and $-y_\infty$ on the boundary:

$$s = 2ly_\infty . \tag{3.21}$$

Note that because y_∞ goes to infinity as we approach to the boundary, the geodesic distance between these two points on the boundary diverges. To obtain the HEE, we need the appropriate variables in the bulk to match the boundary values, which would be the so-called Fefferman-Graham coordinates or simply the Poincarè ones in our case. Hence, we introduce cut-off $\frac{1}{\varepsilon}$ along the radial direction in the bulk in terms of the coordinates r as:

$$\frac{r}{L} = \frac{1}{\varepsilon} . \tag{3.22}$$

From (2.17), one can also obtain the asymptotic behavior of y_∞:

$$\sinh\frac{Lx}{\ell^2} \simeq \varepsilon\sqrt{f(y_\infty) - 1} \simeq \frac{(1 - 2\gamma^2)^{\frac{1}{4}}}{2}e^{y_\infty} . \tag{3.23}$$

This gives

$$y_\infty = \ln\frac{1}{\varepsilon} + \ln\left[2\sinh\frac{2\pi x}{\beta}\right] + \frac{1}{2}\ln\frac{1}{\sqrt{1 - 2\gamma^2}} + \mathcal{O}(\varepsilon) , \tag{3.24}$$

where we used (2.18). Note that the geodesic distance has $2\ell\ln\frac{1}{\varepsilon}$ divergence as $\varepsilon \to 0$. Hence, we subtract this divergence to define the renormalized geodesic distance s_R. Then, the entanglement entropy of the interval $[-x, x]$ on the boundary is found to be

$$S_{HEE} = \frac{s_R}{4G} = \frac{c}{3}\ln\left[2\sinh\frac{2\pi x}{\beta}\right] + \frac{c}{6}\ln A , \tag{3.25}$$

---

[1]Recall that Figure 2 is a constant t slice and the blue line denotes the constant μ curve which is identical with the constant ρ curve.

where we used $c = \frac{3\ell}{2G}$ together with A given in Eq. (2.22). Note that the last term corresponds to the contribution of the boundary entropy, and its small γ expansion reads

$$S_{HEE} \simeq \frac{c}{3} \ln \left[2 \sinh \frac{2\pi x}{\beta} \right] + \frac{c\gamma^2}{6} + \mathcal{O}(c\gamma^4) \,, \tag{3.26}$$

which agrees with (3.14).

4 Entanglement of double RL intervals

In this section, we provide some details about the HEE from the (doubled) RL intervals on the two-sided Janus black holes reviewed in Sec. 2. As is done in the previous section, the HEE can be obtained by the geodesic distance in this case, too. For the geodesics connecting the R and L sides of Janus black holes, we will focus on the constant time slice $\tau = constant$ in the following form of the metric

$$ds^2 = \ell^2 \left[\mathrm{d}y^2 + f(y) \left(\mathrm{d}q^2 - \cosh^2 q \mathrm{d}\tau^2 \right) \right] \,, \tag{4.1}$$

where $f(y)$ was introduced in (2.4) and the AdS$_2$ part is taken by the metric form given in (2.5). In the following, we consider a single geodesic whose boundary position is taken by the same coordinate values as (x, t) with $x > 0$ on the R and L sides, first (See Fig. 5). And then the double geodesics will be taken into consideration to obtain the relevant HEE. For simplicity, the boundary locations of these double geodesics are taken symmetrically as (x, t) and $(-x, t)$ and they will be called the doubled geodesic.

The geodesic equation in the above (y, q, τ) coordinate system[2] could be integrated as

$$\dot{y}^2 + f = \frac{f^2}{E^2} \,, \qquad \dot{} \equiv \frac{\mathrm{d}}{\mathrm{d}q} \,, \tag{4.2}$$

where E is an integration constant and it turns out to be related to the boundary position of the geodesic. This form of the geodesic equation can be integrated in terms of the incomplete elliptic integral of the first kind, as

$$q - q_0 = \frac{A+B}{E} \int_{y_{min}}^{y_{max}} \frac{dy}{\sqrt{\cosh 2y + A} \sqrt{\cosh 2y - B}} = \sqrt{A} \sqrt{m} F(\varphi \,|\, m) \,, \tag{4.3}$$

where q_0 is another integration constant[3] and $y_{min} = \frac{1}{2}\mathrm{arccosh}\, B$. Here, the constant A is introduced before in Eq. (2.22) and the constants B and m are defined, respectively, by

$$B \equiv \frac{2E^2 - 1}{\sqrt{1 - 2\gamma^2}} \,, \qquad m \equiv \frac{2(A+B)}{(A+1)(B+1)} \,, \tag{4.4}$$

---

[2] One easy way to deduce this expression may utilize the Hamiltonian conservation of the Lagrangian $L = \sqrt{\dot{y}^2 + f(y)}$.

[3] This constant q_0 will be dropped in the following, since it could be set to zero by shifting the origin of the coordinates.

13

while the so-called amplitude φ denotes

$$\sin \varphi \equiv \sqrt{\frac{A+1}{2(A+B)}} \, \frac{\sqrt{\cosh 2y_{max} - B}}{\sinh y_{max}} \,. \tag{4.5}$$

Eventually, we will take y_{max} to infinity which corresponds to the position of AdS boundary in these coordinates (See Figure 2 for R/L boundaries which may also be interpreted as denoting constant τ surface with (y, q) coordinates). As usual in the holographic computation, this infinity could be controlled by an appropriate cutoff in the AdS space as in the previous section.

In terms of the geodesic distance s, the geodesic equation could also be written as

$$\dot{s} = \sqrt{\dot{y}^2 + f} = \frac{f}{E} \,. \tag{4.6}$$

Using (4.2) in the above geodesic distance expression and integrating over the y-coordinate, one can deduce that the geodesic distance could be written in terms of the y-coordinate as

$$s - s_0 = \int_{y_{min}}^{y_{max}} dy \frac{\sqrt{\cosh 2y + A}}{\sqrt{\cosh 2y - B}} \,, \tag{4.7}$$

where s_0 is an integration constant[4]. We would like to emphasize that the geodesic distance between R and L boundaries should be twice of the above geodesic distance s with $y_{max} = y_\infty$, since y_{min} could be understood as located in the middle of the R and L boundaries. To see this, it might be useful to recall that the coordinate y is related directly to μ by (2.6).

It is straightforward to integrate the above equation in the form of

$$s = \frac{1}{\sqrt{A+1}\sqrt{B+1}} \left[(A+1)F(\varphi \,|\, m) + (B-1)\Pi(\nu \,;\, \varphi \,|\, m) \right], \qquad \nu \equiv \frac{A+B}{A+1} \,, \tag{4.8}$$

where Π is the incomplete elliptic integral of the third kind, whose properties are summarized in the Appendix A. To proceed in the HEE computation, one needs to introduce the cutoff as in the previous sections. By introducing the cutoff as in (3.22) and using the relation in (3.23) and (3.24), the renormalized geodesic distance can be obtained by removing the cutoff part. To this purpose, consider the behavior of the large $y_{max}(= y_\infty)$ limit as in the previous section. It is straightforward to check, from the integral expression in (4.7), that $s_\infty = y_\infty + finite$ as $\varepsilon \to 0$. Hence, it is useful to introduce $Q(A, B)$ as follows:

$$Q(A, B) = s_\infty - y_\infty + \mathcal{O}\left(\frac{1}{y_\infty}\right), \tag{4.9}$$

---

[4]By taking the origin of the proper distance in such a way that $s = 0$ when $y_{max} = y_{min}$, we set $s_0 = 0$ in the following.

which should be a finite quantity by construction and be independent of the cutoff in the limit of $\epsilon \to 0$ (or $y_\infty \to \infty$). Then, the renormalized geodesic distance, s_R is taken in this case by[5]

$$s_R \equiv \left[s_\infty - \ell \ln \tfrac{1}{\varepsilon} \right]_{\varepsilon \to 0} = \ln 2 \sinh \frac{2\pi x}{\beta} + \frac{1}{2} \ln A + Q(A, B), \qquad (4.10)$$

$$= \ln 2 \cosh \frac{2\pi t}{\beta} + \frac{1}{2} \ln A + Q(A, B) - P(A, B), \qquad (4.11)$$

where P is defined by

$$P(A, B) \equiv \ln \frac{\cosh \frac{2\pi t}{\beta}}{\sinh \frac{2\pi x}{\beta}}. \qquad (4.12)$$

At this stage, one may be perplexed by the notation shown in a such way that P depends on the constants A and B. In fact, this notation is related to the coordinate relations to the q-coordinate or the λ-coordinate as in (2.5) for the boundary position. To see this, recall that the coordinate $y_{max} = y_\infty \to \infty$ is related to the q_∞ coordinate as in (4.3) for geodesics and that the q_∞ (or λ_∞) coordinate is one of the boundary coordinates (see (2.16) and Figure 5). Then, in conjunction with the relation in the asymptotic region given by (2.17), one may set

$$P(A, B) \equiv \ln \sinh q_\infty = \ln \frac{\cosh \frac{2\pi t}{\beta}}{\sinh \frac{2\pi x}{\beta}}, \qquad q_\infty = q_\infty(A, B), \qquad (4.13)$$

where $q_\infty(A, B)$ denotes the boundary position of RL geodesic in such a way that q_∞ itself depends on the constant A and B and so does $P(A, B)$. As will be clear in the following, $P(A, B)$ characterize the approximation for the matching of the bulk expression to boundary results.

Now, we present some steps leading to the elliptic integral representation of $Q(A, B)$. First, note that the argument, $\sin \varphi$ of the incomplete elliptic integrals in (4.8), becomes in the large y_∞ limit

$$\sin \varphi \xrightarrow{y_\infty \to \infty} \sqrt{\frac{A+1}{A+B}} \equiv \sin \varphi_\infty = \frac{1}{\sqrt{\nu}}. \qquad (4.14)$$

In this large y_∞ limit, by using the asymptotic expansion in (A.11), one can also see that

$$R_J(\cos^2 \varphi, \, 1 - m \sin^2 \varphi, \, 1, \, 1 - \nu \sin^2 \varphi)$$

$$= \frac{3\sqrt{(A+B)(B+1)}}{B-1} y_\varepsilon + \left[\frac{3}{2} \frac{1}{\sqrt{xyz}} \ln \frac{2xyz}{(B-1)\sigma^2} + 2R_J(x + \sigma, y + \sigma, z + \sigma, \sigma) \right] + \mathcal{O}(y_\infty e^{-y_\infty}), \qquad (4.15)$$

---

[5]Here, s_∞ corresponds to the half of the (unrenormalized) proper distance of the RL geodesic, since we are taking the integration range of y from $y_{min} = \frac{1}{2}\text{arccosh } B$ to $y_{max} = y_\infty$.

15

where x, y, z and σ are defined as

$$x \equiv \tfrac{B-1}{A+B}, \qquad y \equiv \tfrac{B-1}{B+1}, \qquad z \equiv 1, \qquad \sigma \equiv \sqrt{xy} + \sqrt{yz} + \sqrt{zx}. \qquad (4.16)$$

Finally, using the symmetric elliptic integral[6], one can see that

$$Q(A,B) = \sqrt{\tfrac{A+B}{2}}\sqrt{m}\ F(\varphi_\infty\,|\,m) - \ln\left[\sqrt{\tfrac{B-1}{2}} + \sqrt{\tfrac{A+B}{2}} + \sqrt{\tfrac{B+1}{2}}\right]$$
$$+ \frac{2}{3}\sqrt{xyz}R_J(x+\sigma, y+\sigma, z+\sigma, \sigma), \qquad (4.17)$$

which is a finite expression, indeed. Note also that

$$q_\infty(A,B) = \sqrt{A}\sqrt{m}F(\varphi_\infty\,|\,m) = \sqrt{A}\sqrt{m}R_F\left(\tfrac{B-1}{A+1}, \tfrac{A+B}{A+1}\tfrac{B-1}{B+1}, \tfrac{A+B}{A+1}\right), \qquad (4.18)$$

which justifies our notation $P(A,B)$ in the above since this reveals the dependence on A and B, explicitly.

Though we have obtained the closed form of the relevant quantities in terms of the bulk constants[7] A and B (or equivalently constants γ and E), it is quite involved to compute the HEE in this form. Rather than the bulk constants, the HHE needs to be described by the renormalized geodesic distance related to the appropriate boundary position. In our case, the relevant boundary position needs to be written in terms of boundary coordinates (t,x) in (2.15), not in terms of A and B. In order to represent q_∞ and $Q(A,B)$ in terms of these boundary quantities, it is quite useful to consider some limiting regimes. To this purpose, let us consider two regimes $q_\infty \ll 1$ and $q_\infty \gg 1$, respectively. In these regimes, one can rewrite the expressions, for instance $Q(A,B)$, in terms of q_∞ instead of B. In later sections, one will encounter the same regimes from the boundary ICFT consideration. On the other hand, from the asymptotic expansion of the symmetric elliptic integrals, the useful limiting regimes correspond to the cases of $B \gg A-1$ and $A \gg B-1$. In the following, we show that the appropriate regimes could be obtained from the limiting cases in the symmetric elliptic integral expressions.

• **Regime 1**: $q_\infty \ll 1$

This regime will turn out to be related to the limiting case of bulk constants $B \gg A-1$. First, note that $F(\varphi_\infty|m)$ reduces, in this bulk limit, to

$$F(\varphi_\infty|m) = \sqrt{\tfrac{A+1}{B+1}}R_F(\tfrac{B-1}{B+1}, \tfrac{B-1}{B+1}, 1) + \mathcal{O}(\tfrac{A-1}{B+1}) = \sqrt{\tfrac{A+1}{2}}\ln\left[\sqrt{\tfrac{B+1}{B-1}} + \sqrt{\tfrac{2}{B-1}}\right] + \mathcal{O}(\tfrac{A-1}{B+1}), \qquad (4.19)$$

---

[6]See Appendix A for some details of symmetric elliptic integrals.

[7]Recall that A is the parameter for the Janus background geometry and B is the one for the geodesic.

16

where we used (A.6) and (A.7). Secondly, by using (A.9) and (A.7), the R_J expression reduces to

$$\frac{2}{3}\sqrt{xyz}R_J(x+\sigma, y+\sigma, z+\sigma, \sigma) = \ln\left[1 + 2\sqrt{\tfrac{B+1}{B-1}}\right] - \sqrt{\tfrac{B+1}{2}}\ln\left[\tfrac{\sqrt{B+1}+\sqrt{2}}{B-1}\right] + \mathcal{O}(\tfrac{A-1}{B+1}). \quad (4.20)$$

As a result, $Q(A, B)$ becomes

$$Q(A, B) = \ln\sqrt{\tfrac{2}{B-1}} + \mathcal{O}(\tfrac{A-1}{B+1}). \quad (4.21)$$

And, the expression of q_∞, given by $y_\infty \to \infty$ in (4.3), reduces to

$$q_\infty = \sqrt{A}\ln\left[\sqrt{\tfrac{B+1}{B-1}} + \sqrt{\tfrac{2}{B-1}}\right] + \mathcal{O}(\tfrac{A-1}{B+1}), \quad (4.22)$$

which leads to

$$\sinh\frac{q_\infty}{\sqrt{A}} = \sqrt{\tfrac{2}{B-1}} + \cdots, \quad (4.23)$$

where $\cdots$ denotes the exponentially small part in terms of $\frac{A-1}{B+1}$. It is clear that the $q_\infty \ll 1$ regime corresponds to the $B \gg 1$ case. In the limiting case of $B \gg A - 1$, together with $P(A, B) = \ln\sinh q_\infty$, one obtains

$$Q(A, B) - P(A, B) = \ln\frac{\sinh\frac{q_\infty}{\sqrt{A}}}{\sinh q_\infty} + \cdots. \quad (4.24)$$

As a result, one can see, through (4.11), that the renormalized geodesic distance becomes

$$s_R = \ln 2\cosh\frac{2\pi t}{\beta} \qquad \text{for} \quad q_\infty \ll 1. \quad (4.25)$$

● **Regime 2**: $\underline{q_\infty \gg 1}$

This regime turns out to be correspondent to the case of $A \gg B - 1$. In this bulk limit, one may notice that $m \to \frac{2}{B+1} + \mathcal{O}(\tfrac{B-1}{A+1})$ and $\sin\varphi_\infty = 1 + \mathcal{O}(\tfrac{B-1}{A+1})$ and so that the expression of q_∞ becomes

$$q_\infty = \sqrt{\tfrac{2A}{B+1}}\,\mathbf{K}(\sqrt{\tfrac{2}{B+1}}) + \mathcal{O}(\tfrac{B-1}{A+1}). \quad (4.26)$$

Since the R_J expression reduces to

$$\frac{2}{3}\sqrt{xyz}R_J(x+\sigma, y+\sigma, z+\sigma, \sigma) = \mathcal{O}\left(\tfrac{B-1}{\sqrt{A+1}}\right), \quad (4.27)$$

one can see that

$$Q(A, B) = \sqrt{\tfrac{A+1}{B+1}}\,\mathbf{K}(\sqrt{\tfrac{2}{B+1}}) - \ln\left[\sqrt{\tfrac{B+1}{2}} + \sqrt{\tfrac{B-1}{2}} + \sqrt{\tfrac{A+1}{2}}\right] + \mathcal{O}\left(\tfrac{B-1}{\sqrt{A+1}}\right). \quad (4.28)$$

17

More useful information could be obtained by taking a more specific case as $A \gg 1$ or $B \to 1$. In these cases, one can see that $q_\infty \gg 1$ and so $P(A, B) = \ln \sinh q_\infty \simeq q_\infty - \ln 2$. In each case of $A \gg 1$ and $B \to 1$, the renormalized proper distance is given by

$$
s_R = \begin{cases} \frac{1}{\sqrt{2}} \ln 2 \cosh \frac{Lt}{\ell^2} + (1 - \frac{1}{\sqrt{2}}) \ln \sinh \frac{Lx}{\ell^2} + \frac{3}{2} \ln 2, & \text{for} \quad A \gg 1 \\ \sqrt{\frac{A+1}{2A}} \ln 2 \cosh \frac{Lt}{\ell^2} + \frac{1}{2} \ln A + (1 - \sqrt{\frac{A+1}{2A}}) \ln \sinh \frac{Lx}{\ell^2} - \ln \frac{1 + \sqrt{\frac{A+1}{2}}}{2}, & \text{for} \quad B \to 1 \end{cases} .
$$
(4.29)

It is interesting to observe that the above two regimes might be approached in a simple way by taking $\underline{B = A\alpha \ \& \ A \gg 1}$. In this special case, one may note that the parameter m in (4.4) reduces as $m \to \frac{1+\alpha}{\alpha} \frac{2}{A}$. Using (4.3), (A.7) and (A.12), one can see that

$$
q_\infty = \sqrt{2} \sqrt{\frac{1+\alpha}{\alpha}} \arcsin \frac{1}{\sqrt{1+\alpha}} .
$$
(4.30)

Note also that (4.17), (A.9) and (A.7) lead to

$$
Q(A, B) = \frac{1}{\sqrt{\alpha}} \arcsin \frac{1}{\sqrt{1+\alpha}} - \ln \sqrt{\frac{1+\alpha}{2} A} .
$$
(4.31)

In each case of $\alpha \gg 1$(**regime 1**) and $\frac{1}{A} \ll \alpha \ll 1$ (**regime 2**), one can obtain the s_R expression in terms of the boundary variables by using the above expressions, which reproduce the same forms of the expression in (4.25) and the upper line expression in (4.29), respectively. It is amusing to observe that the final results remain the same, although apparently different-looking functions appear through the different limiting procedures.

Before going ahead, one may consider the case of $A \to 1$, which could also be analyzed in a definite analytic form by using (4.24). In this case, the renormalized proper distance is given by

$$
s_R = \ln 2 \cosh \frac{2\pi t}{\beta} + \frac{1}{2} \ln A + \cdots, \qquad \text{for} \quad A \to 1 .
$$
(4.32)

In fact, one may obtain some analytic form beyond this $A \to 1$ limit. From (4.7), one may notice that

$$
\tfrac{\partial}{\partial A} Q(A, B) = \tfrac{\partial}{\partial A} s = \int_{y_{min}}^{y_\varepsilon} \frac{dy}{\sqrt{\cosh 2y + A} \sqrt{\cosh 2y - B}} \bigg|_{\varepsilon \to 0} = \frac{1}{2} \sqrt{\frac{m}{2(A+B)}} \, F(\varphi_\infty \,|\, m) .
$$
(4.33)

Then, the next order of $A = 1 + \gamma^2 + \mathcal{O}(\gamma^4)$ in the expansion of $Q(A, B)$ could be obtained explicitly as

$$
Q(A, B) = Q(1, B) + \frac{\gamma^2}{2} \sqrt{\frac{m}{2(A+B)}} \, F(\varphi_\infty \,|\, m) + \mathcal{O}(\gamma^4) ,
$$
(4.34)

and the expression of q_∞ in (4.3) becomes

$$
q_\infty = \operatorname{arctanh} \sqrt{\tfrac{2}{B+1}} + \frac{\gamma^2}{8} \left[\sqrt{\tfrac{2}{B+1}} + (4 - \tfrac{B-1}{B+1}) \operatorname{arctanh} \sqrt{\tfrac{2}{B+1}} \right] + \mathcal{O}(\gamma^4) .
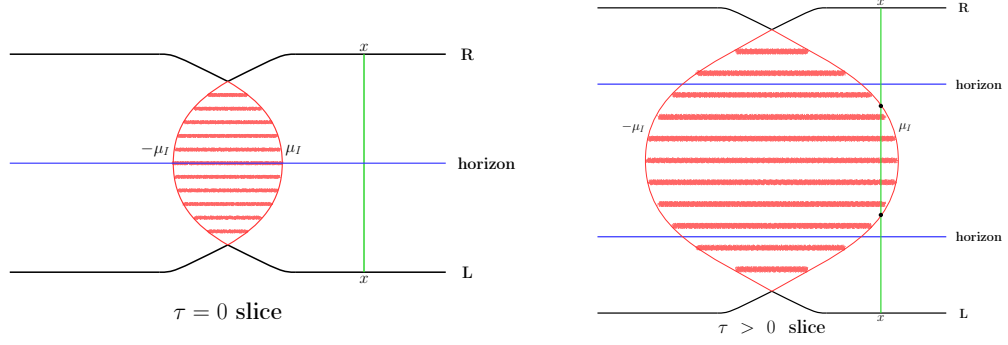$$
(4.35)

18

Figure 5: We have depicted the RL geodesic at $\tau = 0$ and at a later time $\tau > 0$. Though we have depicted the the constant τ slice, the curve $\mu = \pm\mu_I$ takes nearly the same form as in Figure 2.

As before, one could see that $P(A,B) = \ln \sinh q_\infty = \ln \sqrt{\frac{2}{B-1}} + \mathcal{O}(\gamma^2)$ from the above expression and then one obtains

$$Q(A,B) - P(A,B) = \frac{\gamma^2}{8}\left[-1 + \left(\sqrt{\frac{2}{B+1}} - 3\sqrt{\frac{B+1}{2}}\right)\text{arctanh}\sqrt{\frac{2}{B+1}}\right] + \mathcal{O}(\gamma^4). \qquad (4.36)$$

Hence, the renormalized geodesic distance is given by

$$\begin{aligned}
s_R &= \ln 2\cosh\frac{2\pi t}{\beta} + \frac{\gamma^2}{8}\left[3 + \left(\sqrt{\frac{2}{B+1}} - 3\sqrt{\frac{B+1}{2}}\right)\text{arctanh}\sqrt{\frac{2}{B+1}}\right] + \mathcal{O}(\gamma^4), \\
&= \ln 2\cosh\frac{2\pi t}{\beta} + \frac{\gamma^2}{8}\left[3 + \frac{1}{2}\left(\frac{\cosh\frac{2\pi t}{\beta}}{\sqrt{\sinh^2\frac{2\pi x}{\beta} + \cosh^2\frac{2\pi t}{\beta}}}\right.\right. \\
&\qquad \left.\left. - 3\frac{\sqrt{\sinh^2\frac{2\pi x}{\beta} + \cosh^2\frac{2\pi t}{\beta}}}{\cosh\frac{2\pi t}{\beta}}\right)\ln\frac{\sqrt{\sinh^2\frac{2\pi x}{\beta} + \cosh^2\frac{2\pi t}{\beta}} + \cosh\frac{2\pi t}{\beta}}{\sqrt{\sinh^2\frac{2\pi x}{\beta} + \cosh^2\frac{2\pi t}{\beta}} - \cosh\frac{2\pi t}{\beta}}\right] + \mathcal{O}(\gamma^4),
\end{aligned}$$
$$(4.37)$$

where we used $P(A,B) = \ln\sqrt{\frac{2}{B-1}} + \mathcal{O}(\gamma^2)$.

In the limit of $x \gg \frac{\beta}{2\pi}$, the RL geodesic may be drawn as a straight line, since the interface does not deform the shape of the geodesic significantly away from the BTZ limit. It is instructive to observe that the coordinate (y, q) grid or equivalently (μ, w) grid expands as time τ goes on. The growth of the shadow region, as time goes on, could be understood by this behavior of the coordinates in conjunction with the shadow region determination formula in (2.27). Of course, this growth of the shadow region is reminiscent of the growth of the spatial region inside the horizon along the time evolution. See Figure 5. The physical position in the boundary is denoted by x in this figure. At the initial time $\tau = 0$ under $x \gg \frac{\beta}{2\pi}$, the straight line geodesic resides outside of the shadow region. However, as the time goes on, the shadow region becomes larger and so

the geodesic crosses eventually the boundary curve, which is given by μ_I, of the shadow region.

As was explained in the previous section, HEE could read simply from the renormalized geodesic distance and the expression of HEE in the RL geodesic case becomes

$$S_{HEE} = \frac{c}{6} \times 2s_R = \frac{c}{3}s_R\,, \tag{4.38}$$

where the factor 2 comes from the fact that the geodesic distance between R and L boundaries is twice of our expression of s in (4.7). Furthermore, the final expression of the HEE for the region $\mathcal{B}_L \cup \mathcal{B}_R$ (See Figure 7) should be multiplied by another factor 2, since we have considered the symmetric doubled geodesic of the same length in the $+$ and $-$ sides. See the next section for a further interpretation of this doubled geodesic for the HEE.

5 Unitarity, Page curve and Mutual Information

As is well-known, unitarity is one of the fundamental ingredients in quantum mechanics and the famous information loss problem in black hole physics is the clash between the unitarity requirement and a semi-classical computation upon the black hole geometry. Some time ago, Page has sharpened the clash by showing that the entanglement entropy of Hawking radiation (or that of black hole) should follow the so-called Page curve while the semi-classical Hawking's computation tells us that the radiation is thermal and so it cannot follow the curve. The interesting picture on the behavior of the entanglement entropy for eternal black holes was given in [37]. Furthermore, very recent developments in this story [20, 21] is to explain the Page curve by unveiling missing part in the previous semi-classical reasoning and computation. In particular, the island picture has been constructed [25] and explicitly checked in eternal black holes [40].

In this section, we provide some interpretation of the results in the previous sections on the entanglement entropy for three-dimensional Janus black holes. Basically, our interpretation is similar to that of [37], but there are some complication and new aspect, because of the Janus deformation or the ICFT. The RR or LL geodesics corresponds to the entanglement entropy viewed from one side while tracing out the other side, which is time-independent as given in (3.25). The additional term depending on γ in these expressions, which turn out temperature-independent, corresponds to the additional entanglement entropy from the interface QM degrees of freedom. We interpret this as meaning that the additional contribution is nothing to do with the radiation and comes solely from the Janus deformation. This seems natural since the interface QM degrees of freedom are

20

frozen and cannot be escaped from their location contrary to the black hole degrees of freedom.

On the other hand, the RL geodesic corresponds to time-dependent entanglement entropy of the radiation. The late time behavior of this entropy given in (4.25), (4.29) and (4.38) becomes linear and corresponds to the usual deviation from the Page curve. As was explored and explained in [37], the prescription in HEE tells us that the actual entanglement entropy should be taken by the minimum among the extremal ones in the bulk. Therefore, the time-dependent part (or RL geodesic) dominates at the initial stage of the black hole evaporation, while the time-independent one (or RR/LL geodesics) becomes dominant after the Page time. This transition of HEE configuration in the bulk is interpreted as the consequence of the existence of the entanglement islands in eternal black holes [25, 40–42]. In the case of our Janus deformed black holes, there are some additional features which are related to the Janus deformation given by the parameter γ. As shown in (4.29) and (4.37), the location of the geodesic on the R/L boundary, denoted simply by x, from the angled-joint $x = 0$ appears in the entanglement entropy expression, which vanishes in the limit of $A \to 1$, *i.e.* in the BTZ limit. We would like to interpret this γ-dependent contribution as the entanglement between the interface QM degrees of freedom and those in the outside of the location x in CFT[8]. This entanglement is also time independent and there is the interplay of this entanglement with the radiation entanglement. We would like to interpret the LR geodesic expression as representing the entanglement transfer between the initial entanglement of the interface to the black hole and that to the radiation.

It is also interesting to observe that the behavior of the entanglement entropy before the Page time depends on the parameter γ. We have depicted schematically the Page curve in Figure 6.

According to the minimum choice prescription in the HEE, the Page time could be taken as the time when the RR/LL HEE in (3.25) and the RL HEE in (4.10) become equal. Note also that the integration constant B is related to the boundary time t (and the position $x = L_0/2$ in our setup) through (4.13). This tells us that one may write $B = B(t)$. This consideration leads to the following expression for the Page time

$$Q(A, B(t_P)) = 0. \tag{5.1}$$

To obtain some explicit expression of the Page time, let us consider the case $A \gg B - 1$ with $A \gg 1$ or the case $B = Aa$ & $A \gg 1$ & $a \ll 1$. In these limits, one can see that

---

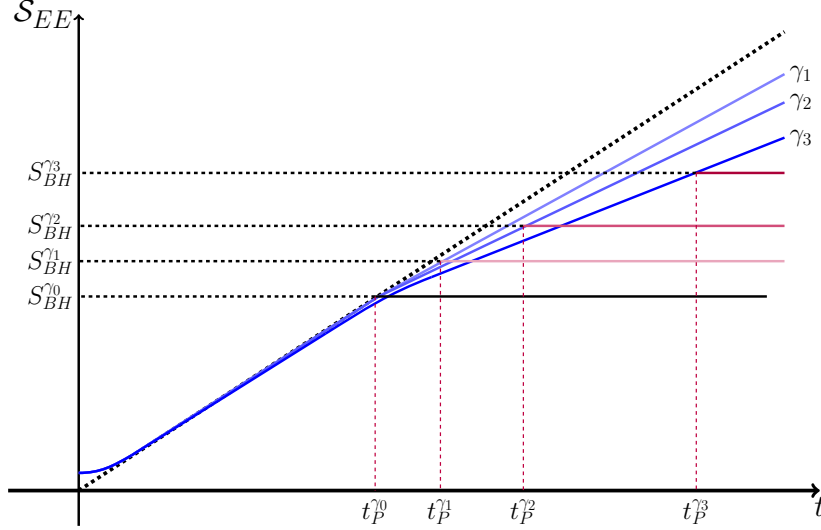[8]There are two outsides in CFT_- and CFT_+.

Figure 6: We have depicted the Page curves for the parameters $\gamma_1 < \gamma_2 < \gamma_3$.

$Q(A, B) = 0$ condition leads to

$$\ln \sinh q_\infty = \frac{1}{\sqrt{2}} \ln \frac{A}{2} - \ln 2 \,. \tag{5.2}$$

For the large separation and the Page time $t_P, L_0 \gg 1$, one obtains

$$t_P \simeq \frac{L_0}{2} + \frac{1}{\sqrt{2}} \ln \frac{A}{2} - \ln 2 \,, \tag{5.3}$$

which tells us that the Page time becomes larger as the γ (or A) gets bigger. This aspect is also depicted in Figure 6.

Before going ahead, let us consider the information transfer from black holes to radiations in our setup. Basically, this discussion is similar to the information transfer in the eternal BTZ black holes [37, 40] but there are additional features because of the interface degrees of freedom. For a concrete discussion, let us denote the interval of our interest as $\mathcal{B}$ and its complement $\bar{\mathcal{B}}$, which corresponds to the black holes and radiations, respectively in the two-dimensional gravity viewpoint. Our setup corresponds to the two-sided black holes and so it becomes a quadripartite system, $\mathcal{B}_R \cup \mathcal{B}_L \cup \bar{\mathcal{B}}_R \cup \bar{\mathcal{B}}_L$. The radiation parts may be further decomposed into the $\pm$ part as $\bar{\mathcal{B}}_{R/L} = \bar{\mathcal{B}}^+_{R/L} \cup \bar{\mathcal{B}}^-_{R/L}$ in each R/L side, respectively, in this two dimensional case (See Figure 7). For simplicity, we consider the $+/-$ symmetric case with a R/L symmetric evolution.

As the initial configuration we have taken the TFD state as in (2.24), which tells us the maximal entanglement between R and L sides and that the quadripartite state, as a whole,
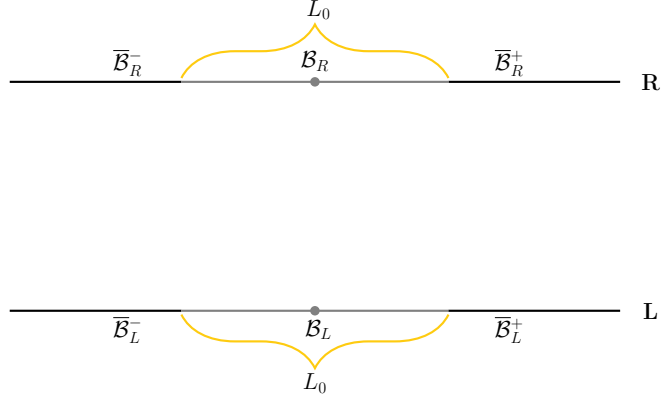
22

Figure 7: In this figure, our entanglement configuration is illustrated.

is a pure state. In this setup, we begins with a large entanglement between $\mathcal{B}_R$ and $\mathcal{B}_L$ and a large entanglement between $\bar{\mathcal{B}}_R$ and $\bar{\mathcal{B}}_L$[9]. This could be achieved by taking a large length limit of the interval $\mathcal{B}$ as $\frac{2\pi}{\beta}L_0 \gg 1$. In this limit, the initial entanglement between $\mathcal{B}_R$ and $\bar{\mathcal{B}}_R$ ($\mathcal{B}_L$ and $\bar{\mathcal{B}}_L$) becomes very small and so we may ignore this contribution. This initial setup may be phrased in terms of the mutual information as

$$I(\mathcal{B}_R, \bar{\mathcal{B}}_R)(t=0) = I(\mathcal{B}_L, \bar{\mathcal{B}}_L)(t=0) \simeq 0 \,. \tag{5.4}$$

Recall that the entanglement entropy $S(\mathcal{B}_R) = S(\mathcal{B}_L)$ of the interval of the length L_0 can be obtained holographically by RR or LL geodesics as given in (3.25), which is time-independent. Likewise, the entropy $2S(\bar{\mathcal{B}}_R^+ \cup \bar{\mathcal{B}}_L^+) = 2S(\bar{\mathcal{B}}_R^- \cup \bar{\mathcal{B}}_L^-) = S(\bar{\mathcal{B}}_R \cup \bar{\mathcal{B}}_L) = S(\mathcal{B}_R \cup \mathcal{B}_L)$ may be thought to be obtained by the doubled RL geodesic given in (4.38). However, this should be taken carefully, since the correct HEE should be taken as the minimum among the geodesics, as was done in the above Page curve consideration. On this regard, one may rephrase one version of the information paradox [37, 44] for eternal black holes in terms of the mutual information. The mutual information of $\mathcal{B}_R$ and $\mathcal{B}_L$ is given by

$$I(\mathcal{B}_R, \mathcal{B}_L) = S(\mathcal{B}_R) + S(\mathcal{B}_L) - S(\mathcal{B}_R \cup \mathcal{B}_L) \,. \tag{5.5}$$

If $S(\mathcal{B}_R \cup \mathcal{B}_L)$ is blindly taken by the doubled RL geodesic, the mutual information would become negative after the Page time, which gives us a contradiction since it cannot be negative (subadditivity). In other words, the non-negative property of the mutual information insists us that it should be zero after the Page time and so the initial large entanglement between $\mathcal{B}_R$ and $\mathcal{B}_L$ disappears after the Page time. In fact, we know that

---

[9]For another initial entanglement case, see Ref. [43].

23

the correct $S(\mathcal{B}_R \cup \mathcal{B}_L)$ needs to be taken by the combination of the RR and LL geodesics, as done in the above. Concretely, one can obtain the explicit expression of $I(\mathcal{B}_R, \mathcal{B}_L)$ from our bulk results as

$$I(\mathcal{B}_R, \mathcal{B}_L)(t) = -\frac{2c}{3}Q\Big(A, B(t)\Big). \tag{5.6}$$

Indeed, one can see the large initial mutual information given, since we have taken $L_0 \gg \beta$, by

$$I(\mathcal{B}_R, \mathcal{B}_L)(t=0) = -\frac{2c}{3}Q\Big(A, B(t=0)\Big) = \frac{2c}{3}\ln\sinh\frac{\pi L_0}{\beta} + \frac{c}{3}\ln A. \tag{5.7}$$

Now, one may wonder where the large initial entanglement goes after the Page time. To see this, let us note that $S(\bar{\mathcal{B}}_{R/L})$ could also be obtained by a RR or LL geodesic and that it would be time-independent. Then, in conjunction with RL symmetry one may see that $I(\mathcal{B}_R, \bar{\mathcal{B}}_R) = I(\mathcal{B}_L, \bar{\mathcal{B}}_L)$ is also time-independent, since the entanglement entropy of one side to the other, $S(\mathcal{B}_R \cup \bar{\mathcal{B}}_R) = S(\mathcal{B}_L \cup \bar{\mathcal{B}}_L)$, is time-independent in the TFD construction. Recalling that $I(\mathcal{B}_R, \bar{\mathcal{B}}_R) = I(\mathcal{B}_L, \bar{\mathcal{B}}_L)$ was taken as vanishing small from the start, one may note that $B_{R/L}$ would be nearly disentangled from $\bar{B}_{R/L}$ at any time. By dividing the quadripartite state to bipartite ones, we can see that

$$S(\bar{\mathcal{B}}_R) = S(\mathcal{B}_L \cup \bar{\mathcal{B}}_L \cup \mathcal{B}_R) = S(\mathcal{B}_R) + S(\mathcal{B}_L \cup \bar{\mathcal{B}}_L) - I(\mathcal{B}_R, \mathcal{B}_L \cup \bar{\mathcal{B}}_L)$$
$$= S(\mathcal{B}_R) + S(\mathcal{B}_L) + S(\bar{\mathcal{B}}_L) - I(\mathcal{B}_L, \bar{\mathcal{B}}_L) - I(\mathcal{B}_R, \mathcal{B}_L \cup \bar{\mathcal{B}}_L), \tag{5.8}$$

which leads to, together with RL symmetry,

$$2S(\mathcal{B}_R) = 2S(\mathcal{B}_L) = I(\mathcal{B}_L, \bar{\mathcal{B}}_L) + I(\mathcal{B}_R, \mathcal{B}_L \cup \bar{\mathcal{B}}_L) \simeq I(\mathcal{B}_R, \mathcal{B}_L \cup \bar{\mathcal{B}}_L). \tag{5.9}$$

The purity of the whole state $\mathcal{B}_R \cup \bar{\mathcal{B}}_R \cup \mathcal{B}_L \cup \bar{\mathcal{B}}_L$ with the nearly disentanglement of $\mathcal{B}_R$ from $\bar{\mathcal{B}}_R$ would lead to the nearly maximal entanglement of $\mathcal{B}_R$ with $\mathcal{B}_L \cup \bar{\mathcal{B}}_L$, which implies

$$I(\mathcal{B}_R, \mathcal{B}_L \cup \bar{\mathcal{B}}_L) \simeq I(\mathcal{B}_R, \mathcal{B}_L) + I(\mathcal{B}_R, \bar{\mathcal{B}}_L) \simeq 2S(\mathcal{B}_R) = 2S(\mathcal{B}_L). \tag{5.10}$$

Now, one can see that the decrease of $I(\mathcal{B}_R, \mathcal{B}_L)$ leads to the increase of $I(\mathcal{B}_R, \bar{\mathcal{B}}_L)$ while their sum remains constant. As a result, the large initial entanglement between $\mathcal{B}_R$ and $\mathcal{B}_L$ transferred to the one between $\mathcal{B}_R$ and $\bar{\mathcal{B}}_L$ (or R $\leftrightarrow$ L vice versa). This tells us in our setup the information transfer between $\mathcal{B}$ and $\bar{\mathcal{B}}$.

6 Outside-horizon description of 2d gravities

In this section, we would like to discuss the 2d gravity description of the interface degrees. Our description here will be mainly based on a straightforward reinterpretation of the 3d

bulk description. Especially from the bulk perspectives, the 2d gravity theories $\mathrm{Grav}_\pm$ are induced at the $\pm\mu_I$ surfaces by integrating out 3d bulk degrees over the region $[-\mu_I, \mu_I]$. Of course these theories are dependent upon the choice of $\pm\mu_I$ in general. However any choices will be equivalent to one another since the resulting theories are introduced by hand from the view point of the original 3d bulk theory. Namely the descriptions are related with one another simply by some field redefinition of their dynamical degrees[10]. Hence our value μ_I in (2.27) will be just one possibility, which was chosen for the sake of our convenience.

The $\pm\mu_I$ theories are in general interacting with each other, which is rather clear from the bulk point of view since there are bulk degrees connecting the two parts. The relevant interaction strength is governed by the geodesic distance between the two surfaces which is of order $\ln A$. Indeed one may check that interaction terms are suppressed as $1/\ln A$. Hence in the large $\ln A$ limit, the two theories are effectively decoupled from each other. Of course for small γ (or $A \sim 1$), there is no decoupling at all and the two theories are rather strongly coupled from each other.

To see the nature of these induced theories, note first the metric solutions for $\mathrm{Grav}_\pm$ are simply given by AdS_2 with

$$ds_\pm^2 = \left[-(w_\pm^2 - 1)\frac{(2\pi)^2}{\beta^2}dt^2 + \frac{dw_\pm^2}{w_\pm^2 - 1} \right] \ell_2^2, \qquad (6.1)$$

where $\ell_2 = \ell\sqrt{f(\pm\mu_I)}$. These are nothing but the induced metrics of the $\pm\mu_I$ surfaces from the 3d bulk metric. We shall view that these metrics are following from some Jackiw-Teitelboim (JT) gravities [18, 19] involving a large extra potential for the 2d dilaton as well as the 2d scalar field originated from our 3d scalar field ϕ. In the large $\ln A$ limit, we shall assume that the pure gravity part becomes almost non-dynamical with the AdS_2 metric while leaving only the topological contribution $k_0 \int R_2$[11]. Of course some 2d matters can be dynamical and propagating in this AdS_2 background.

To check this explicitly, let us consider a single-sided boundary-to-boundary extremal curve starting from $(-x_-, t)$ ending on (x_+, t) where we take $x_\pm > 0$ such that the shadow region is included along its trajectory. As drawn in Figure 8, this entangling geodesic cuts the $\pm\mu_I$ surfaces at $(w_\pm, t)$ respectively where $w_\pm$ will be a function of $x_\pm$ in general. When γ is small, it is clear that $w_+(x_\pm) = w_-(x_\pm) + O(\gamma^2)$, which shows that $\mathrm{Grav}_\pm$ are strongly coupled from each other.

---

[10]This statement can be made precise in the framework of holographic renormalization [45].

[11]A posteriori, one may partly justify this assumption by the consistency of our 2d description with the original 3d counter part as described below. Its full justification is beyond scope of the present work. Further investigation on this issue will be given elsewhere.
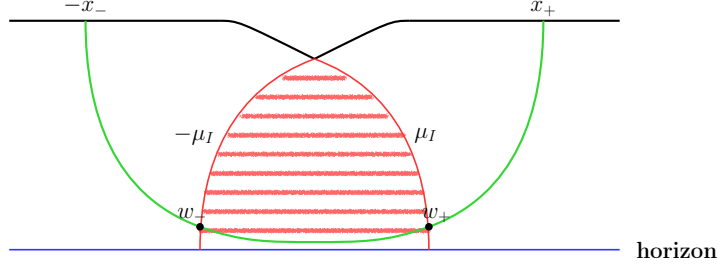
Figure 8: We draw here a single-sided boundary-to-boundary extremal geodesic curve starting from $(-x_-, t)$ ending on (x_+, t). This entangling geodesic cuts the $\pm\mu_I$ surfaces at $(w_\pm, t)$ respectively.

When A becomes large, the values $w_\pm$ induced on the $\pm\mu_I$ surfaces approach $w_{\pm\infty}$ as

$$w_\pm = w_{\pm\infty}(x_\pm) + O(1/\ln A),\tag{6.2}$$

with the boundary values $w_{\pm\infty}(x_\pm) = \coth\frac{2\pi}{\beta}x_\pm$. To show this, we first note that the relevant geodesic equations in (3.18) can be integrated to give

$$\rho(y) = 2\mathcal{E}\int_0^y dy \frac{A}{\sqrt{\cosh 2y + A}\sqrt{\cosh 2y + A - 2A\mathcal{E}^2}},$$

$$s(y) = \int_0^y dy \frac{\sqrt{\cosh 2y + A}}{\sqrt{\cosh 2y + A - 2A\mathcal{E}^2}},\tag{6.3}$$

together with $t = constant$. In order to make the geodesic stay outside horizon, we will require $\mathcal{E}^2 < \frac{1}{2}(1 + 1/A)$. Further assuming $\mathcal{E} \ll 1$, we may expand the above expressions with respect to $\mathcal{E}$ leading to

$$\rho_\infty - \rho_{-\infty} = 4\mathcal{E}\mathcal{Q}(A) + O(\mathcal{E}^3),$$

$$s_\infty - s_{-\infty} = y_\infty - y_{-\infty} + 2\mathcal{E}^2\mathcal{Q}(A) + O(\mathcal{E}^4),\tag{6.4}$$

where

$$\mathcal{Q}(A) \equiv \int_0^\infty dy \frac{A}{\cosh 2y + A} = \frac{1}{2}\ln 2A + O(A^{-2}).\tag{6.5}$$

Therefore, the integration constant $\mathcal{E}$ can be fixed as

$$\mathcal{E} = \frac{\rho_\infty - \rho_{-\infty}}{4\mathcal{Q}(A)} + O(\mathcal{E}^3),\tag{6.6}$$

and the corresponding renormalized geodesic distance becomes

$$s_R = \ln A + \ln 2\sinh\frac{2\pi}{\beta}x_+ + \ln 2\sinh\frac{2\pi}{\beta}x_- + \frac{(\rho_\infty - \rho_{-\infty})^2}{8\mathcal{Q}(A)} + O(\mathcal{E}^4),\tag{6.7}$$

26

where $\cosh\rho_{\pm\infty} = \coth\frac{2\pi}{\beta}x_{\pm}$. Thus one finds our assumption $\mathcal{E} \ll 1$ is fulfilled for any finite choice of $x_{\pm}$ since the factor $\mathcal{Q}(A)$ in the denominator of (6.6) becomes large when A becomes large enough. We conclude that the resulting entanglement entropy for the interval $[-\mathbf{x}_-, \mathbf{x}_+]$ becomes

$$S = S_{(+)}(x_+) + S_{(-)}(x_-) + O(1/\ln A), \qquad (6.8)$$

where

$$S_{(\pm)}(x_{\pm}) = \frac{c}{6}\ln 2\sinh\frac{2\pi}{\beta}x_{\pm} + S_I^{(\pm)}, \qquad (6.9)$$

with $S_I^{(+)} + S_I^{(-)} = S_I$. This shows an effective decoupling of the $(+)$ and $(-)$ theories when $\ln A \gg 1$. However the decoupling has a subtlety since the interface degrees will be shared by the $(+)$ and $(-)$ theories at the same time. At the moment one may regard the interface contributions $S_I^{(\pm)}(\geq 0)$ to be arbitrary once their sum is fixed to be S_I. To complete our discussion here, we now compute the differences

$$\rho_{\pm\infty} - \rho(\pm y_I) = \pm\frac{\rho_{\infty} - \rho_{-\infty}}{2\mathcal{Q}(A)}\mathcal{Q}_I(A) + O(\mathcal{E}^3), \qquad (6.10)$$

where the coordinate values $\pm y_I$ again referring to the $\pm$ surfaces are defined by $\pm y_I = y(\pm\mu_I)$ and

$$\mathcal{Q}_I(A) \equiv \int_{y_I}^{\infty} dy \frac{A}{\cosh 2y + A} = 1 + O(A^{-2}). \qquad (6.11)$$

Therefore the differences are of order $1/\ln A$, which demonstrates our claim in (6.2). The resulting values $w_{\pm}(x_{\pm})$ may be considered as on-shell solutions of the $\text{Grav}_{\pm}$ theories. Since $\text{Grav}_{\pm}$ are coupled to $\text{CFT}_{\pm}$ and $x_{\pm}$ represent coordinate values in $\text{CFT}_{\pm}$, the above result strongly suggests that $\text{Grav}_+/\text{Grav}_-$ is coupled only to $\text{CFT}_+/\text{CFT}_-$ respectively. Hence we concludes that $\text{Grav}_+ \times \text{CFT}_+$ and $\text{Grav}_- \times \text{CFT}_-$ are effectively decoupled from each other as $\ln A \gg 1$. Below we shall focus on the nature of the $(\pm)$ theories in the limit $\ln A \gg 1$ safely ignoring any possible interactions between them.

We posit here one possible description of $\text{Grav}_{\pm} \times \text{CFT}_{\pm}$ for the region outside horizon, which is based on straightforward re-interpretation of our 3d bulk computation. We shall check our proposal in various limiting cases later on. For the $(+)$ theory of $\text{Grav}_+ \times \text{CFT}_+$, we choose the following coordinate system. We first introduce spatial coordinate $a_{\pm} > 0$ by $w_{\pm} = \coth\frac{2\pi}{\beta}a_{\pm}$ in the gravity side. For the AdS Rindler wedge of the black hole spacetime, let us introduce coordinates $\sigma_{(+)}^{\pm} = t \mp a_+$ with a restriction $\sigma_{(+)}^+ < \sigma_{(+)}^-$. The metric in (6.1) becomes

$$ds_{(+)}^2 = -\frac{d\sigma_{(+)}^+ d\sigma_{(+)}^-}{\sinh^2\frac{\pi}{\beta}(\sigma_{(+)}^+ - \sigma_{(+)}^-)}\left(\frac{2\pi\ell_2}{\beta}\right)^2. \qquad (6.12)$$

For the flat spacetime region of CFT$_+$, we introduce the coordinates by $\sigma^\pm_{(+)} = t \pm x_+$ with the flat metric

$$ds^2_{(+)} = -d\sigma^+_{(+)}d\sigma^-_{(+)}\,, \tag{6.13}$$

with the range $\sigma^+_{(+)} > \sigma^-_{(+)}$. These two charts are joined through the surface $\sigma^+_{(+)} = \sigma^-_{(+)}$ and then the whole coordinate range of $(\sigma^+_{(+)}, \sigma^-_{(+)})$ covers the entire planar region of $\mathbb{R}^2$.

For the $(-)$ theory, one has $\sigma^\pm_{(-)} = t \pm a_-$ for the black hole part with the restriction $\sigma^+_{(-)} > \sigma^-_{(-)}$ and $\sigma^\pm_{(-)} = t \mp x_-$ for the flat space of CFT$_-$ with $\sigma^+_{(-)} < \sigma^-_{(-)}$. The metric in the black hole/the flat region is respectively given by (6.12)/(6.13) with all the subscripts $(+)$ replaced by $(-)$.

We assume that our original CFT matters (with the central charge c) on the flat region of the 2d spacetime is extended into the outside-horizon region of the black hole spacetime[12]. This determines basically the coupling between Grav$_+$ and CFT$_\pm$. Recall that our pure gravity part is solely given by the topological contribution. The total topological contribution is non-dynamical and shared by Grav$_+$ and Grav$_-$. In this sense, the $(\pm)$ theories do not decouple from each other completely.

With this preliminary, the generalized entropy for the interval $[-a_+, x_+] \cup [-x_-, a_-]$, which includes quantum matter contribution, can be identified as [40]

$$S_{\text{gen}}(a_\pm, x_\pm) = S_+(a_+, x_+) + S_-(a_-, x_-)\,, \tag{6.14}$$

where

$$S_{(\pm)}(a_\pm, x_\pm) = \frac{c}{6} \ln \frac{2\sinh^2 \frac{\pi}{\beta}(a_\pm + x_\pm)}{\sinh \frac{2\pi}{\beta}a_\pm} + S^{(\pm)}_I\,. \tag{6.15}$$

Note that $S^{(\pm)}_I$ are from the topological contribution of pure gravity part.

6.1 Some checks

Let us now justify the above expression of the generalized entropy. First of all, its extremization with respect to $a_\pm$ leads to the conditions

$$\coth\frac{\pi}{\beta}(a_\pm + x_\pm) = \coth\frac{2\pi}{\beta}a_\pm\,. \tag{6.16}$$

Their solutions are simply given by

$$a_\pm = x_\pm\,, \tag{6.17}$$

---

[12] As will be clarified in Section 8, they may be further extended into the behind-horizon region excluding any such region where extra AdS$_2$ matters are excited.

which lead to the quantum extremal entropies

$$S_{\text{ext}}^{(\pm)} = \frac{c}{6} \ln 2 \sinh \frac{2\pi}{\beta} x_\pm + S_I^{(\pm)} \,. \tag{6.18}$$

The solutions and the resulting extremal entropies perfectly agree with those from the 3d gravity in (6.2) and (6.8). Thus we check the validness of the 2d description at least on-shell.
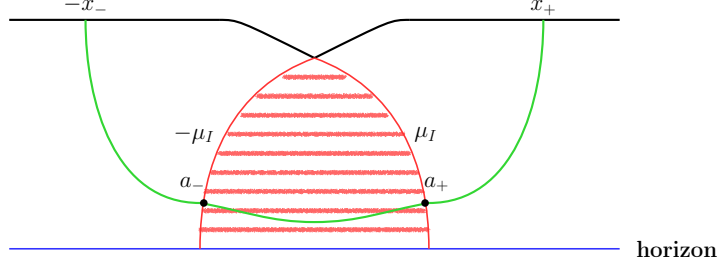

Figure 9: In this figure, we depict an off-shell configuration where one connects (x_+, t) to (a_+, t), (a_+, t) to (a_-, t), and (a_-, t) to $(-x_-, t)$ with each segment connected extremally.

We now check the generalized entropy in (6.14) at its off-shell level. For this let us consider an off-shell configuration where one connects (x_+, t) to (a_+, t) on the $+\mu_I$ surface, (a_+, t) to (a_-, t) on the $-\mu_I$ surface, and (a_-, t) to $(-x_-, t)$ with each segment connected extremally. See its illustration in Figure 9. The configuration in total will be geodesic when $a_\pm = x_\pm + O(1/\ln A)$ as mentioned previously. For each segment, we apply the solution in (6.3) by matching the starting and the ending values of ρ coordinate, which will fix the integration constant $\mathcal{E}$ uniquely. We first consider the case where $\frac{2\pi}{\beta} x_\pm \gg 1$ and $\frac{2\pi}{\beta} a_\pm \gg 1$. In this case, one finds that $\mathcal{E} \ll 1$ for each segment and the solution in (6.3) can be expanded in $\mathcal{E}$ as was done previously. For the extremal curve connecting $(a_\pm, t)$ to $(\pm x_\pm, t)$, we note that

$$\rho_{\pm\infty} = 2e^{-\frac{\pi}{\beta} x_\pm} + O(e^{-\frac{3\pi}{\beta} x_\pm}) \,,$$
$$\rho(\pm y_I) = 2e^{-\frac{\pi}{\beta} a_\pm} + O(e^{-\frac{3\pi}{\beta} a_\pm}) \,, \tag{6.19}$$

and then

$$\mathcal{E} = \frac{e^{-\frac{\pi}{\beta} x_\pm} - e^{-\frac{\pi}{\beta} a_\pm}}{\mathcal{Q}_I(A)} + O\left[\left(e^{-\frac{\pi}{\beta} x_\pm} + e^{-\frac{\pi}{\beta} a_\pm}\right)^3\right] \,. \tag{6.20}$$

The resulting renormalized extremal distance becomes

$$s_{a_\pm \to x_\pm} = \frac{1}{2} \ln A - y_I + \ln 2 \sinh \frac{2\pi}{\beta} x_\pm + \frac{(e^{-\frac{\pi}{\beta} x_\pm} - e^{-\frac{\pi}{\beta} a_\pm})^2}{\mathcal{Q}_I(A)} + O\left[\left(e^{-\frac{\pi}{\beta} x_\pm} + e^{-\frac{\pi}{\beta} a_\pm}\right)^4\right] \,. \tag{6.21}$$

29

The extremal distance from (a_-, t) to (a_+, t) can also be computed in a similar way leading to

$$s_{a_- \to a_+} = 2y_I + \frac{(e^{-\frac{\pi}{\beta}a_+} - e^{-\frac{\pi}{\beta}a_-})^2}{\mathcal{Q}_{-+}(A)} + O\left[\left(e^{-\frac{\pi}{\beta}a_+} + e^{-\frac{\pi}{\beta}a_-} \right)^4 \right] , \tag{6.22}$$

where

$$\mathcal{Q}_{-+}(A) \equiv \int_{-y_I}^{+y_I} dy \frac{A}{\cosh 2y + A} . \tag{6.23}$$

The first term in this expression is independent of $a_\pm$ and gives the topological contribution of S_I if one includes the constant terms of the remaining segments. Noting

$$\mathcal{Q}_{-+}(A) = \ln A + \cdots , \tag{6.24}$$

one may ignore the second term of (6.22) in the limit $\ln A \gg 1$. Therefore one finds the total contribution to the generalized entropy becomes

$$S_{\text{tot}} = S_{\text{gen}}(a_\pm, x_\pm) + O\left[\left(e^{-\frac{\pi}{\beta}a_+} + e^{-\frac{\pi}{\beta}a_-} \right)^2 / \ln A \right] + O\left[\left(e^{-\frac{\pi}{\beta}a_+} + e^{-\frac{\pi}{\beta}a_-} + e^{-\frac{\pi}{\beta}x_\pm} \right)^4 \right] . \tag{6.25}$$

Hence we have an agreement with (6.14) ignoring the higher order correction terms. Finally we consider the off-shell configuration where $a_\pm = x_\pm + \delta a_\pm$ but with no further assumption on $x_\pm > 0$. It is straightforward to show that

$$S_{\text{tot}} = S_{\text{gen}}(x_\pm + \delta a_\pm, x_\pm) + O(\delta a_\pm^2 / \ln A) + O(\delta a_\pm^4) . \tag{6.26}$$

Hence, one has again a perfect agreement with (6.14) up to the order of $\delta a_\pm^2$.

7 ICFT description of entanglement entropy

Before going on, we would like to explain the ICFT computation of the entanglement entropy and its relation to our HEE in the previous sections rather schematically[13]. The main object we are interested in is the reduced density matrix $\rho_{\mathcal{II}}$ of the Janus TFD state (2.25) over the RL intervals $\mathcal{II} \equiv \mathcal{I}_L \cup \mathcal{I}_R = [-\mathbf{x}_-, \mathbf{x}_+]_{\mathbf{L}} \cup [-\mathbf{x}_-, \mathbf{x}_+]_{\mathbf{R}}$ at time $t_L = t_R = t \geq 0$. As before, the trace of its n-th power can be computed using the R/L twist operators by

$$\text{tr}\rho_{\mathcal{II}}^n = \langle \Phi_{nR}^+(t, x_+) \Phi_{nR}^-(t, -x_-) \Phi_{nL}^+(t, -x_-) \Phi_{nL}^-(t, x_+) \rangle_{\text{JTFD}} . \tag{7.1}$$

Then the corresponding entanglement entropy is given by

$$S_{\mathcal{II}}^{EE}(t) = -\lim_{n \to 1} \frac{\partial}{\partial n} \text{tr}\rho_{\mathcal{II}}^n . \tag{7.2}$$

---

[13]We are working with our Janus ICFT which has the corresponding dual gravity description. Therefore, note that some results in this section depend on the microscopic details of underlying AdS/CFT correspondence.

The above four-point function on the Janus TFD can be mapped to a four-point correlation function on a single $\mathbb{R}^2$ by the exponential map [37]

$$\pm X^\pm = e^{\pm \frac{2\pi}{\beta} x_{R/L}^\pm} \,. \tag{7.3}$$

where

$$\begin{aligned}
x_R^\pm &= t \pm x \,, \\
x_L^\pm &= -\left(t + \frac{\beta}{2} i\right) \pm x \,.
\end{aligned} \tag{7.4}$$

Namely the trace in (7.1) can be mapped to

$$\mathrm{tr}\rho_{\mathcal{II}}^n = \langle \Phi_n^+(X_1^\pm) \Phi_n^-(X_2^\pm) \Phi_n^+(X_3^\pm) \Phi_n^-(X_4^\pm) \rangle_{\mathrm{ICFT}} \,. \tag{7.5}$$

with

$$\begin{aligned}
x_1^\pm &= t \pm x_+ \,, \\
x_2^\pm &= t \pm (-x_-) \,, \\
x_3^\pm &= -\left(t + \frac{\beta}{2} i\right) \pm (-x_-) \,, \\
x_4^\pm &= -\left(t + \frac{\beta}{2} i\right) \pm x_+ \,,
\end{aligned} \tag{7.6}$$

where the expectation value of operators is taken over the ICFT vacuum state on $\mathbb{R}^2$. Hence the HEE computation of Sections 4 and 5 should be understood as the above four-point function with the choice $x_+ = x_- = x > 0$. In this case, the remaining $SO(2,1)$ symmetries of the ICFT dictates the general form of the four-point function to be

$$\mathrm{tr}\rho_{\mathcal{II}}^n|_{x_\pm = x} = \frac{1}{\left(2 \sinh \frac{2\pi}{\beta} x\right)^{4\Delta_n}} \left(G_n(\xi)\right)^2 \,, \tag{7.7}$$

where ξ is the cross ratio given by

$$\xi = \frac{\cosh^2 \frac{2\pi}{\beta} t}{\sinh^2 \frac{2\pi}{\beta} x} \,. \tag{7.8}$$

The $Q(A,B)$ function of HEE side defined over $0 \le \xi \le \xi(t_P)$ is then related to G_n by

$$\frac{c}{3} \left[Q\left(A, B(\xi)\right) + \ln \sqrt{A} \right] = -\lim_{n \to 1} \frac{\partial}{\partial n} G_n(\xi) \,, \tag{7.9}$$

where $B(\xi)$ is defined by the relation $\xi = \sinh^2 q_\infty(A,B)$ together with $q_\infty(A,B)$ in (4.18). The $\xi \to 0$ limit is the so-called bulk OPE limit where the presence of our interface can be ignored. Namely, when $\xi \ll 1$, one has

$$G_n \simeq G_0 \, \xi^{-\Delta_n} \,, \tag{7.10}$$

31

where G_0 is an n-independent constant, which basically follows from the bulk OPE limit since the inserted points are relatively far away from the interface and thus the presence of the interface can be safely ignored. From this, one may recover the small ξ behavior

$$S^{EE}_{\mathcal{II}} \simeq \frac{2c}{3} \ln 2 \cosh \frac{2\pi}{\beta} t \,, \tag{7.11}$$

which agrees with our HEE result given in (4.25) and (4.38). On the other hand, the transition occurs at $t = t_P$ and, when $\xi \geq \xi(t_P)$, the corresponding expression of $[G_n]^2$ in the strongly coupled regime becomes

$$\left[G_n(\xi)\right]^2 = \widetilde{G}_0^2 \, A^{\frac{c}{3}(1-n)} \,, \tag{7.12}$$

whose n-dependence is determined from the HEE expression in (3.25). The A dependence is from the interface identity operator where $e^{\frac{c}{3}(1-n)\ln A}$ is from the degeneracy factor of the interface ground states in the replica n copy of the ICFT. In the intermediate region of $0 \leq \xi \leq \xi(t_P)$, the detailed dynamics of RL extremal curve plays a role, which was discussed briefly in Sections 4 and 5. In the limit $A \to 1$, the interface degrees disappear completely and one regains the full conformal symmetries out of $SO(2,1)$. In this case, the behavior in (7.11) will be valid over the full region of $0 \leq \xi \leq \xi(t_P)$ if one assumes the large c limit of holographic theories [37].

Below we shall be mainly concerned with the large deformation limit $\ln A \gg 1$ with general $x_\pm \gg \beta$. In this case, we again have an effective ($\pm$) separation of the Janus TFD theory. Namely, one has an effective factorization[14]

$$\mathrm{tr}\rho^n_{\mathcal{II}} \simeq \langle \Phi^+_{nR}(t, x_+)\Phi^-_{nL}\rangle_{\mathrm{TFD}} \, \langle \Phi^-_{nR}(t, -x_-)\Phi^+_{nL}(t, -x_-)\rangle_{\mathrm{TFD}} \,. \tag{7.13}$$

The resulting ($\pm$) dynamics has the interpretation of $\mathrm{Grav}_\pm \times \mathrm{CFT}^R_\pm \times \mathrm{CFT}^L_\pm$ respectively. Further each ($\pm$) theory has a corresponding BCFT interpretation where some part of the interface degrees play role of boundary degrees. Again the ($\pm$) two-point functions have general forms

$$\langle \Phi^+_{nR}(t, \pm x_\pm)\Phi^-_{nL}(t, \pm x_\pm)\rangle_{\mathrm{TFD}} = \frac{1}{\left(2\sinh \frac{2\pi}{\beta}x_\pm\right)^{2\Delta_n}} G^{(\pm)}_n(\xi_\pm) \,, \tag{7.14}$$

where the ($\pm$) cross ratios are respectively given by

$$\xi_\pm = \frac{\cosh^2 \frac{2\pi}{\beta}t}{\sinh^2 \frac{2\pi}{\beta}x_\pm} \,. \tag{7.15}$$

---

[14]This factorization fails in a subtle manner when $t \geq t_P$ because the interface degrees are shared by the ($\pm$) theories. We shall clarify this subtlety later on.

Then, our $Q(A, B)$ function of the HEE side defined over $0 \leq \xi_\pm \leq \xi_\pm(t_P)$ is again related to $G_n^{(\pm)}$ by

$$\frac{c}{3}\left[Q(A, B(\xi_\pm)) + \ln \sqrt{A}\right] = -\lim_{n \to 1} \frac{\partial}{\partial n} G_n^{(\pm)}(\xi_\pm). \tag{7.16}$$

However, as we shall clarify below, there remain some subtle dynamical correlations between the $(\pm)$ theories since the interface degrees are shared by the $(\pm)$ theories.

8 Islands and behind-horizon dynamics

In this section, we shall be mainly concerned about the behind-horizon dynamics of the region $0 \leq \xi_\pm \leq \xi_\pm(t_P)$, which is described by the RL extremal curves holographically. We again assume $\ln A \gg 1$ such that one may trust our 2d gravity description of the $(\pm)$ theories. In this section, we shall omit any possible corrections of order $1/\ln A$ for the simplicity of our presentation.

First, let us describe the spacetime picture of $\text{Grav}_\pm \times \text{CFT}_\pm^R \times \text{CFT}_\pm^L$. We present here the case of the $(+)$ theory and the $(-)$ theory can be treated exactly in a parallel manner. Below we basically follow the reference [40]. Let us begin by introducing two copies of $\mathbb{R}^2$ coordinates $\sigma_R^\pm = t_R \pm x_R$ and $\sigma_L^\pm = -t_L \pm x_L$ covering R/L AdS$_2$ Rindler wedge for $x_{R/L} < 0$ joined to the R/L flat spacetime $x_{R/L} > 0$. The metric for the R/L Rindler wedge is given by

$$ds_{R/L}^2 = -\frac{d\sigma_{R/L}^+ d\sigma_{R/L}^-}{\sinh^2 \frac{\pi}{\beta}(\sigma_{R/L}^+ - \sigma_{R/L}^-)} \left(\frac{2\pi\ell_2}{\beta}\right)^2, \tag{8.1}$$

for the region $\sigma_{R/L}^+ < \sigma_{R/L}^-$ and the one for the R/L flat region $\sigma_{R/L}^+ > \sigma_{R/L}^-$ by

$$ds_{R/L}^2 = -d\sigma_{R/L}^+ d\sigma_{R/L}^-. \tag{8.2}$$

Those two regions in each set are joined along $\sigma_{R/L}^+ = \sigma_{R/L}^-$ as described by vertical lines in Figure 10.

The above two copies of $\mathbb{R}^2$ can be mapped to a single $\mathbb{R}^2$ with coordinates $U^\pm$ by the exponential map, $U^\pm = \pm e^{\pm \frac{2\pi}{\beta}\sigma_R^\pm}$ and $U^\pm = \mp e^{\pm \frac{2\pi}{\beta}\sigma_L^\pm}$ [40]. The R/L flat regions specified by $U^+ U^- < -1$ have the metric

$$ds^2 = \frac{dU^+ dU^-}{U^+ U^-}\frac{\beta^2}{4\pi^2}, \tag{8.3}$$

whereas the two-sided black hole spacetime specified by $-1 < U^+ U^-$ has the metric

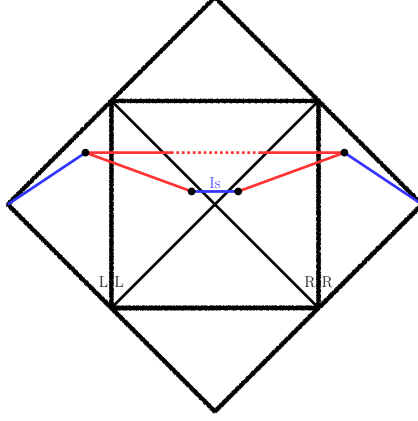$$ds^2 = -\frac{4dU^+ dU^-}{(1 + U^+ U^-)^2}\ell_2^2. \tag{8.4}$$

33

Figure 10: We draw the Penrose diagram of the full 2d spacetime. One two-sided AdS$_2$ black hole is joined to the R/L flat regions of $\sigma^+_{R/L} > \sigma^-_{R/L}$ along $\sigma^+_{R/L} = \sigma^-_{R/L}$. The upper R/L point has coordinates $(t_{R/L}, x_{R/L}) = (t, x_+)$ with our choice. As was shown in Section 6, before extremization, the lower R/L point has coordinates $(t, -a_{R/L})$, which will be fixed to be $(t, -x_\pm)$ after extremization. The bule line denoted by "Is" is for the island configuration.

In this coordinate system, $U^+U^- = -1$ is the joint of the black hole and the R/L flat regions.

As was mentioned already, at $t = t_P$, there will be a transition from the LR connecting extremal curves to the LL/RR extremal curves in the bulk side. After the transition, the bulk picture is given in Figure 11. The time slice of the configuration is chosen as follows; except the island plus its bulk extension which is in the constant τ slice, all the remaining regions are in constant t slice. The green curves represent the relevant part of
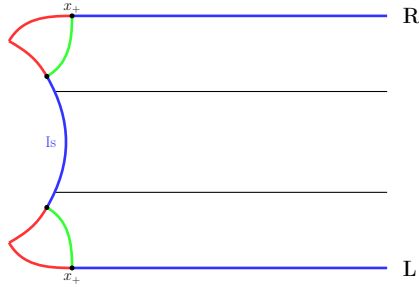

Figure 11: The bulk picture is given for $t \geq t_P$. The time slice of the configuration is chosen as follows; Except the island plus its bulk extension, which is in the constant τ slice, all the remaining regions are in constant t slice. The green-colored curves represent the bulk extremal curves and the blue curve denoted by "Is" is for the island configuration.

LL/RR bulk extremal curves. The 2d boundary of the relevant bulk spacetime is given in Figure 10. In this 2d picture, the whole configuration after the page time consists of two

34

blue curves connecting $(t, \infty)_{R/L}$ and $(t, x_+)_{R/L}$, two red curves connecting $(t, x_+)_{R/L}$ and $(t, -a_{R/L})_{R/L}$ and so-called island curve connecting $(t, -a_R)_R$ and $(t, -a_L)_L$. In Section 6, we have shown that the corresponding generalized entropy in (6.14) is minimized with $a_{L/R} = x_+$. The bulk extremal curves are then represented by the two red curves connecting $(t, x_+)_{R/L}$ and $(t, -x_+)_{R/L}$ as depicted in Figure 10. Note that, except the island which is along the corresponding constant τ slice, all the remaining curves are along the constant t slice upon extremization. Adding the contribution of the $(-)$ theory, we have

$$S_{\mathcal{II}} \quad = \quad S_{(+)} + S_{(-)}, \tag{8.5}$$

$$S_{(\pm)}(t \geq t_P) \quad = \quad \frac{c}{3} \ln 2 \sinh \frac{2\pi}{\beta} x_\pm + S_I^{(\pm)}, \tag{8.6}$$

where the topological contributions $S_I^{(\pm)}$ are constrained by $S_I^{(+)} + S_I^{(-)} = 2S_I$ as was explained before. We shall specify the values of $S_I^{(\pm)}$ later on.

Since the full two dimensional theories are unitary, one may alternatively obtain $S_{(+)}$ by the QES including island contribution [40]

$$S_{(+)} = \min \text{ext} \left[S_I^{(+)} + S_{[x_+, \infty)_L \cup [x_+, \infty)_R \cup Is}^{\text{matter}} \right], \tag{8.7}$$

where the topological term $S_I^{(+)}$ is the geometric contribution from the end points of the island and the second term from the 2d matter contribution of the relevant intervals. (Of course, one has a parallel story for the $(-)$ theory.) Therefore we conclude that the island is formed after the Page time and the degrees in the island region are entangled with radiation of the region $[x_+, \infty)_R \cup [x_+, \infty)_L$. Since the island is connected to the radiation through the 3d bulk, the development of entanglement between them seems rather clear. Also note that the island contribution should be included in the original ICFT computation of the entanglement entropy of the intervals $[\mathbf{x_+}, \infty)_\mathbf{L} \cup [\mathbf{x_+}, \infty)_\mathbf{R} \cup (-\infty, -\mathbf{x_-}]_\mathbf{L} \cup (-\infty, -\mathbf{x_-}]_\mathbf{R}$. Hence, its appearance is solely due to our effective 2d gravity description.

We now explain how this entanglement is developed in time. It will be mainly accounted by the behind-horizon dynamics of the RL extremal curves in the region $0 \leq \xi_\pm \leq \xi_\pm(t_P)$. As was mentioned, the dynamics of QES before the transition is rather complicated, whose details are mainly based on our holographic computation of the RL extremal curves. It basically shows how degrees in $[-\mathbf{x_-}, \mathbf{x_+}]_\mathbf{L} \cup [-\mathbf{x_-}, \mathbf{x_+}]_\mathbf{R}$, which in particular include the R/L interface degrees, are entangled with the rest (called as radiation) as time goes by. The first is the so-called bulk OPE limit where $\xi_+ \ll 1$, i.e. the RL extremal curve is relative far away from the surface $\mu = \mu_I$. We depict the corresponding configuration on the left side of Figure 12. In this regime, one has

$$S_{\mathcal{II}} = S_{(+)} + S_{(-)}, \tag{8.8}$$

where

$$S_{(\pm)} = \frac{c}{3} \ln 2 \cosh \frac{2\pi}{\beta} t + O(\xi_\pm) \,. \tag{8.9}$$

For the entire region before the transition $0 \leq \xi_+ < \xi_+(t_P)$, the contribution from the (green-colored) bulk extremal curve can be recovered from the red-colored region which is connecting $(t, x_+)_R$ to $(t, x_+)_L$ through the black hole spacetime as depicted in Figure 12. The corresponding curve is also depicted in Figure 10 by the single red line connecting $(t, x_+)_R$ to $(t, x_+)_L$. In the bulk OPE limit of $\xi_+ \ll 1$, the contribution from the interface degrees can be ignored and the original CFT matter of central charge c will be responsible for the dynamics even including behind-horizon region. This contribution has been identified in [40], which precisely agrees with the expression in (8.9). See Appendix B for its detailed computation using the two-point function of the twist operators.
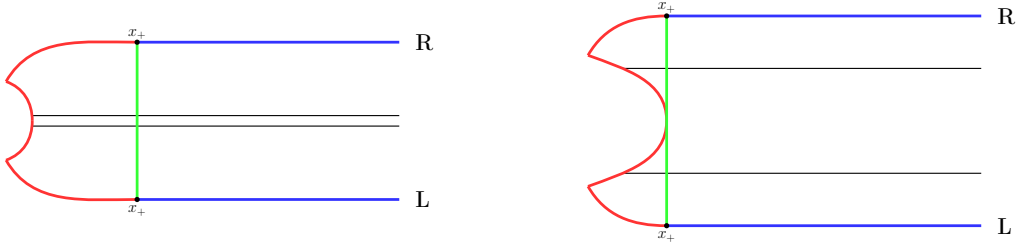

Figure 12: The 3d bulk picture of constant τ slice is given for $0 \leq \xi_+ \leq \xi_I$. On the left side, we draw the RL extremal curve with $\xi_+ \ll 1$. On the right side we depict the RL extremal curve just touching the $\mu = \mu_I$ surface.

In this bulk OPE limit, the form of $G_n^{(\pm)}$ is known to have a general form

$$G_n^{(\pm)} \simeq G_0 \, \xi_\pm^{-\Delta_n} \,, \tag{8.10}$$

which is a straightforward generalization of (7.10). Of course the entanglement entropy in (8.9) is then followed from the formula (7.16) and (8.10).

We now turn to general holographic expression valid for the region $0 \leq \xi_\pm \leq \xi_\pm(t_P)$ with $\ln A \gg 1$. The corresponding behaviors are basically described by (4.30) and (4.31). In terms of $\xi_\pm$, $S_{(\pm)}$ is identified as

$$S_{(\pm)} = \frac{c}{3} \left(\ln 2 \sinh \frac{2\pi}{\beta} x_\pm + \frac{\ln \left(\sqrt{\xi_\pm} + \sqrt{\xi_\pm + 1} \right)}{\sqrt{2}\sqrt{1+\alpha_\pm}} - \frac{1}{2} \ln \frac{1+\alpha_\pm}{2} \right), \tag{8.11}$$

where $\alpha_\pm$ is related to $\xi_\pm$ by

$$\ln \left(\sqrt{\xi_\pm} + \sqrt{\xi_\pm + 1} \right) = \frac{\sqrt{2}\sqrt{1+\alpha_\pm}}{\sqrt{\alpha_\pm}} \arcsin \frac{1}{\sqrt{1+\alpha_\pm}} \,. \tag{8.12}$$

36

The small $\xi_\pm$ behavior of (8.9) is following from the regime $\alpha_\pm \gg 1$. Another well known regime of interest is the so-called boundary (interface in our case) OPE limit of $\xi_\pm \gg 1$. The transitional behavior from the bulk to the interface limit occurs around $\xi_\pm = 1$, which corresponds to $\alpha_\pm(\xi_\pm = 1) \simeq 2.83586$. In the regime of $0 \leq \xi_\pm \leq 1$, the radiation of bulk RL entanglement $\ln 2 \cosh \frac{2\pi}{\beta} t$ (via the bulk channel of operator $\Phi_n^\pm$) plays a dominant role. Of course the outgoing and ingoing components are balanced with each other such that the spacetime outside horizon remains stationary[15].

At $\alpha_\pm = \alpha_I = \frac{1}{e^2-1}$, the extremal curves begin to touch the surface $\mu = \pm \mu_I$ where our Grav$_\pm$ is defined respectively. At this point, one has $\xi_\pm = \xi_I \simeq 18841.1$. The corresponding configuration is drawn on the right hand side of Figure 12.
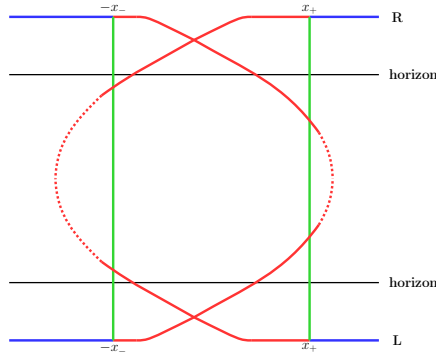

Figure 13: The 3d bulk picture of constant τ slice is given for $\xi_I \leq \xi_\pm \leq \xi_\pm(t_P)$. In this figure, we choose the case $x_+ > x_-$ for the sake of illustration. The dotted red lines represent the behind-horizon regions where the induced AdS_2 matters are excited. On the remaining part of the 2d spacetimes, the original CFT matters of central charge c propagate.

After then one begins to see details of the shadow region. As time goes by, the shadow region behind horizon is getting bigger and bigger as drawn in Figure 13. When $\xi_\pm \gg 1$, the $S_{(\pm)}$ becomes

$$S_{(\pm)} = \frac{c}{3}\left(\ln 2 \sinh \frac{2\pi}{\beta} x_\pm + \frac{1}{\sqrt{2}} \ln \frac{\cosh \frac{2\pi}{\beta} t}{\sinh \frac{2\pi}{\beta} x_\pm} + \frac{1+\sqrt{2}}{2} \ln 2 + O\big((\ln \xi_\pm)^{-2}\big) \right). \quad (8.13)$$

As $\xi_\pm$ is getting bigger, one is probing deeper region of the shadow. This implies that the radiation and the degrees in the deeper region of the shadow are entangled more and more as time goes by. Comparing the above with the entanglement entropy at the Page time in (8.5), one finds the Page time satisfies

$$\ln \xi_+(t_P)\xi_-(t_P) = 2\sqrt{2}\ln A - 2(2+\sqrt{2})\ln 2, \quad (8.14)$$

---

[15]The outgoing and ingoing components of radiation are between $\mathcal{B}_L$ and $\bar{\mathcal{B}}_R$ or between $\mathcal{B}_R$ and $\bar{\mathcal{B}}_L$ in the notation of Section 5.

where we assume $\xi_{\pm}(t_P) \gg 1$ for the simplicity of our presentation. When $x_{\pm} \gg \beta$ and $\ln A \gg |x_+ - x_-|/\beta$, one has a solution

$$t_P = \frac{x_+ + x_-}{2} + \frac{\beta}{4\pi}\left(\sqrt{2}\ln A - (2 + \sqrt{2})\ln 2\right), \tag{8.15}$$

where we ignore any exponentially small corrections.

The entropy $S_{(\pm)}$ developed up to the Page time reads

$$S_{(\pm)}(t_P) = \frac{c}{3}\ln 2\sinh\frac{2\pi}{\beta}x_{\pm} + S_I^{(\pm)}, \tag{8.16}$$

where

$$S_I^{(\pm)} = \frac{c}{6}\left[\mp\sqrt{2}\ln\frac{\sinh\frac{2\pi}{\beta}x_+}{\sinh\frac{2\pi}{\beta}x_-} + \ln A\right]. \tag{8.17}$$

The first term on the right hand side of (8.16) shows the entanglement between the bulk CFT degrees in $[-x_-, x_+]_{R/L}$ and the $(\pm)$ radiation. The remaining term $S_I^{(\pm)}$ represents the entanglement between the interface degrees and the $(\pm)$ radiation respectively. Hence for instance when $x_+ > x_-$, one can see that the $(-)$ radiation ($[-\infty, -x_-]_L \cup [-\infty, -x_-]_R$) is more entangled with the interface degrees than the $(+)$ radiation ($[x_+, \infty]_L \cup [x_+, \infty]_R$). In Figure 13, we draw the shape of the configuration in the regime $\xi_I \le \xi_{\pm} \le \xi_{\pm}(t_P)$ with $x_+ > x_-$. Thus we conclude that the $(+)$ and $(-)$ theories are dynamically correlated with each other even in the limit $\ln A \gg 1$.

The above described behavior in the regime of $\xi \gg 1$ can be summarized in terms of the function $\text{tr}\rho_{\mathcal{II}}^n$ by

$$\text{tr}\rho_{\mathcal{II}}^n \simeq \frac{1}{\left(4\sinh\frac{2\pi}{\beta}x_+ \sinh\frac{2\pi}{\beta}x_-\right)^{2\Delta_n}}\left[G_n^{(\pm)}(\xi_{\pm})G_n^{(\pm)}(\xi_{\pm}) + G_I^2 A^{-\frac{c}{3}(n-1)}\right], \tag{8.18}$$

where

$$G_n^{(\pm)}(\xi_{\pm}) = G_I\left[\sum_k g_{n,k}\xi^{-\hat{\Delta}_{n,k}} + 2^{-(1+\sqrt{2})\delta_n}\xi_{\pm}^{-\hat{\Delta}_n}\right], \tag{8.19}$$

with $\hat{\Delta}_{n,k} > \hat{\Delta}_n$ for $n > 1$, $\hat{\Delta}_{1,k} = \hat{\Delta}_1 = 0$ and $\delta_1 = 0$. Here, G_I is an overall n-independent constant. From our behavior of the entanglement entropy, one finds $\partial_n\delta_n|_{n\to 1} = \sqrt{2}\partial_n\hat{\Delta}_n|_{n\to 1} = \frac{c}{6}$. This form is consistent with the boundary OPE limit in [46, 47]. From this one may find the transition of the entanglement entropy at the Page time t_P in (8.14). It is also consistent with the requirement $\text{tr}\,\rho_{\mathcal{II}} = 1$. To recover (8.13) in the regime $1 \ll \xi_{\pm} \le \xi_{\pm}(t_P)$, we assume the last term in the bracket of (8.19) dominates over the remaining terms once $\xi_{\pm} \gg 1$. It also gives us the desired form of the entanglement entropy in (8.6). The second term in the bracket of (8.18) is from the boundary

OPE from the bulk to interface identity operator. The n-dependence of its coefficient is explained below (7.12). Since the interface degrees are shared by the ($\pm$) theories, the corresponding interface ground states, on which ($\pm$) boundary operators including the interface identity are acting, are shared by the ($\pm$) theories as well. This is the reason why the factorization fails with the interface identity operator in (8.18). It is clear that the assumption of vacuum block dominance in [33] is not respected in our holographic interface theory.

All the above boundary (interface) operators of dimensions $\hat{\Delta}_{n,k}$ and $\hat{\Delta}_n$, which are induced by $\Phi_n^{\pm}$, are responsible for the behind-horizon dynamics of generalized entropy. The corresponding AdS$_2$ matter contribution should be included when we are dealing with the generalized entropy using the 2d gravity theory. For the illustration, see Figures 10 and 13. The dotted red lines represent regions where these extra AdS$_2$ matters propagate. On the remaining part of the 2d spacetime, the original CFT matters of central charge c propagate. The transition between the two occurs roughly where the bulk extremal curves are touching the $\mu = \pm\mu_I$ surfaces.

Based on this observation, we carry out the 2d CFT computation of the generalized entropy $\hat{S}_{\text{gen}}$ in Appendix B. In this 2d setup, we consider the causal diamond D_{RL} defined by the two points $P_{R/L}$ with coordinates $U_R^{\pm} = \pm e^{\frac{2\pi}{\beta}(\pm t+x)} = \tan\frac{\tau\pm\lambda}{2}$ and $U_L^{\pm} = \mp e^{\frac{2\pi}{\beta}(\mp t+x)} = \tan\frac{\tau\mp\lambda}{2}$, respectively. The interval with end points $P_{R/L}$ will be denoted by $\mathcal{I}_{RL}$. We take $x > 0$ and $\pi > \lambda > \frac{\pi}{2}$ such that these points lie in the flat region of Figure 10. We further introduce an interval $\mathcal{I}_{rl}$ specified by two points $P_{r/l}$ with coordinates $U_r^{\pm} = \tan\frac{\tau_0\pm\lambda_0}{2}$ and $U_l^{\pm} = \tan\frac{\tau_0\mp\lambda_0}{2}$, respectively, where we used the left right symmetry of our problem. We require $\frac{\pi}{2} > \lambda_0 \geq 0$ such that the points $P_{r/l}$ lie within the AdS$_2$ region (of the diamond D_{RL}). The induced boundary (interface) operator $\hat{O}_n$ of dimension $\hat{\Delta}_n$ is assumed to be excited within the interval $\mathcal{I}_{rl}$ of the AdS$_2$ region[16]. We further denote the interval defined by $\{P_R, P_r\}/\{P_L, P_l\}$ as $\mathcal{I}_{Rr}/\mathcal{I}_{Ll}$, respectively.

The entanglement entropy $\hat{S}_{Rr}/\hat{S}_{Ll}$ of the interval $\mathcal{I}_{Rr}/\mathcal{I}_{Ll}$ can be evaluated from the two-point function of the twist operators $\Phi_n^{\pm}$ as usual. Similarly the induced contribution $\hat{S}_{rl}$ can be computed from the two-point function $\langle\hat{O}_n(P_r)\hat{O}_n(P_l)\rangle$. We then consider the generalized entropy given by

$$\hat{S}_{\text{gen}} = \hat{S}_{Rr} + \hat{S}_{Ll} + \hat{S}_{rl} = 2\hat{S}_{Rr} + \hat{S}_{rl}, \qquad (8.20)$$

where we set $\hat{S}_{Rr} = \hat{S}_{Ll}$ using the left right symmetry of our problem. In this computation we assume that any possible mutual information between the three intervals can be

---

[16]Upon extremization, the two points $P_{r/l}$ roughly become the end points of each dotted red line in Figures 10 and 13.

ignored. One finds $\tau_0 = \tau$ upon extremization. Hence the extremum is achieved along the constant τ slice which is in accordance with our holographic computation. Upon further extremizing with respect to λ_0, one finds two solutions in the regime $\xi_\pm \gg 1$. Note that the points $P_{r/l}$ in these solutions all lie behind the horizon of AdS$_2$. Another relevant configuration for the entanglement entropy of $\mathcal{I}_{RL}$ is the one without any extra AdS$_2$ matter contribution. This becomes

$$\hat{S}_{RL} = \frac{c}{3} \ln 2 \cosh \frac{2\pi}{\beta} t \,. \tag{8.21}$$

Choosing the minimum among these three and setting $\hat{q} = \frac{1}{\sqrt{2}}$ (See (B.7) for its definition), one finds the entanglement entropy from the 2d perspective as

$$\hat{S}_{(\pm)} = \frac{c}{3} \left[\ln 2 \sinh \frac{2\pi}{\beta} x_\pm + \frac{1}{\sqrt{2}} \ln \frac{2 \cosh \frac{2\pi}{\beta} t}{\sinh \frac{2\pi}{\beta} x_\pm} + 2 \ln 2 - \sqrt{2} \ln(1+\sqrt{2}) + O\big(\xi_\pm^{-1}\big) \right], \tag{8.22}$$

for the regime $\xi_\pm \gg 1$. The details of the computation will be relegated to Appendix B. Note that the above entropy $\hat{S}_\pm$ agrees with our HEE in (8.13) up to constant terms: The difference reads

$$S_{(\pm)} - \hat{S}_{(\pm)} \simeq \frac{c}{3} \left[\sqrt{2} \ln(1+\sqrt{2}) - \frac{3}{2} \ln 2 \right] \simeq 0.069 \, c \,. \tag{8.23}$$

Of course, we do not expect any precise agreement since our discussion is based on number of approximations. In particular the transitional region between the original CFT and the induced AdS$_2$ matter excitation is not so sharply defined in our original HEE configuration in Figure 13.

These behind-horizon matters will be responsible for the outgoing and ingoing components of radiation in the regime $\xi_\pm \gg 1$. Hence the extra AdS$_2$ matters are contributing to the entanglement evolution in the behind-horizon region in addition to the original CFT matter of central charge c. Further study is required in this direction.

9 Conclusions

In this work, we have investigated the entanglement entropy/information evolution of black holes surrounded with radiations from three different perspectives and showed that it follows the anticipated Page curve. Firstly, we have evaluated holographically the entanglement entropy of the boundary intervals by using the geodesic distance in the 3d Janus black holes. Secondly, we have made the boundary ICFT interpretation of this HEE in Janus black holes. And then we provide the effective 2d gravity realization dual to the interface degree of freedom, which is coupled to CFT$_2$. In this reduced gravity,

we have also confirmed that the QES with island picture can reproduce the holographic entanglement entropy computed in 3d gravity. All of these perspectives lead to a consistent picture and confirms the unitary evolution of entanglement entropy.

In the 3d Janus black hole, the conventional Ryu-Takayanagi surface (geodesic in our case) can give the entanglement entropy of two intervals located in the left and right boundary respectively. As usual, the change of the topology of the Ryu-Takayanagi surface leads to the phase transition of the entanglement at the Page time t_P which is increasing as the interface degree of freedom, represented by $\ln A$, gets larger. When the Page time is large enough, we found an additional phase transition before the Page time. This new phase can naturally be understood from the point of view of the effective 2d gravity dual to the interface degrees coupled to CFT_2. As the interface degree of freedom is mixed with CFT_2, the surface where the 2d gravity lives expands. If $\ln A$ is large enough, this surface for the 2d gravity intersects with the Ryu-Takayanagi surface connecting the left and right intervals before the Page time. And, this causes the new phase transition to occur.

When $\ln A$ is sufficiently large, one can view our system as two *nearly decoupled* BCFT. From the BCFT point of view, the entanglement entropy can be evaluated by the two point function of the twist operators. In early time, the bulk OPE channel dominates to the first phase. As time passes, we consider the boundary OPE channel which is mediated by boundary operators on 2d gravity induced by the twist operator. Note that the broken conformal symmetry to $SO(1,2)$ on the 2d gravity leads to the effective conformal dimension of the induced operator. And, this reproduces the second phase obtained by 3d Ryu-Takayanagi surface.

Following the island conjecture, we computed the generalized entropy in the 2d gravity coupled to CFT_2 system, and its extremization agrees with the 3d gravity calculation. Also, for the given points x_+ and $-x_-$ on the CFT_2, we considered geodesic connecting them with $a_\pm$ on the 2d gravity surface (See Figure 9), which was found to agree with the generalized entropy in 2d system. This explains why we need to extremize the generalized entropy to get the correct answer because the geodesic connecting among $\pm x_\pm$ and $a_\pm$ naturally leads to the Ryu-Takayanagi surface in 3d gravity by its extremization with respect to $a_\pm$ by definition of the geodesic.

Our top-down approach in this work can give us concrete answers on the 2d gravities. Starting from 3d Janus black hole for instance, it would be highly interesting to obtain the effective 2d gravity directly by integrating out the bulk degrees. Also, it is intriguing to investigate the entanglement wedge reconstruction. From the point of view of 2d effective gravity coupled to CFT_2, one can study the Petz map which reconstructs operators behind

41

horizon [42] to see the effect of the interface degree of freedom on the reconstruction. And, one might be able to reinterpret the entanglement wedge reconstruction of 2d system from the 3d point of view.

In this work, our study is focused on the entanglement evolution of the 3d Janus black hole. Its higher dimensional generalization will be of interest. It might also be interesting to consider the higher derivative corrections in the gravity action [48] and the flat space adaptation [49].

Acknowledgement

A   Elliptic integrals

In this section, we summarize various formulae about elliptic integrals, which are used in the main text. (See [50] and references therein for a more detailed information about elliptic integrals.) The incomplete elliptic integral of the first kind $F(\varphi\,|\,m)$ is defined as

$$F(\varphi\,|\,m) = \int_0^\varphi \frac{d\theta}{\sqrt{1 - m\sin^2\theta}}\,, \tag{A.1}$$

and the incomplete elliptic integral of the third kind is defined as

$$\Pi(\nu\,;\,\varphi\,|\,m) = \int_0^\varphi \frac{1}{1 - \nu\sin^2\theta}\frac{d\theta}{\sqrt{1 - m\sin^2\theta}}\,. \tag{A.2}$$

These become the complete elliptic integrals in the case of $\varphi = \frac{\pi}{2}$ as

$$\mathbf{K}(k) = F\!\left(\frac{\pi}{2}\,\Big|\,k^2\right), \qquad \mathbf{\Pi}(\nu\,;\,k) = \Pi\!\left(\nu\,;\,\frac{\pi}{2}\,\Big|\,k^2\right). \tag{A.3}$$

The symmetric elliptic integrals are defined as

$$R_F(x,y,z) = \frac{1}{2}\int_0^\infty \frac{dt}{\sqrt{t+x}\sqrt{t+y}\sqrt{t+z}}\,, \tag{A.4}$$

$$R_J(x,y,z,p) = \frac{3}{2}\int_0^\infty \frac{dt}{(t+p)\sqrt{t+x}\sqrt{t+y}\sqrt{t+z}}\,, \tag{A.5}$$

and

$$R_C(x, y) \equiv R_F(x, y, y), \qquad R_D(x, y, z) \equiv R_J(x, y, z, z). \tag{A.6}$$

These symmetric forms are more useful for obtaining the asymptotic expansion and for providing more efficient numerical computation. In particular, the symmetric integral R_C can be written in terms of elementary functions as

$$R_C(x, y) = \begin{cases} \frac{1}{\sqrt{y-x}} \arccos\sqrt{\frac{x}{y}} & , & x < y \\ \frac{1}{\sqrt{x-y}} \mathrm{arccosh}\sqrt{\frac{x}{y}} = \frac{1}{\sqrt{x-y}} \ln \frac{\sqrt{x}+\sqrt{x-y}}{\sqrt{y}} & , & x > y \end{cases}. \tag{A.7}$$

The symmetric forms have the following scaling properties:

$$R_F(\lambda x, \lambda y, \lambda z) = \lambda^{-\frac{1}{2}} R_F(x, y, z), \qquad R_J(\lambda x, \lambda y, \lambda z, \lambda p) = \lambda^{-\frac{3}{2}} R_J(x, y, z, p). \tag{A.8}$$

Another useful relation:

$$R_J(x, y, y, p) = \frac{3}{p-y}\Big[R_C(x, y) - R_C(x, p)\Big], \qquad p \neq y. \tag{A.9}$$

Useful asymptotic expansion formulae in the main text:

$$R_F(x, y, z) = \frac{1}{2\sqrt{z}} \ln \frac{16z}{(\sqrt{x}+\sqrt{y})^2} + \mathcal{O}\Big(\tfrac{x+y}{2}, \sqrt{xy}\Big) \qquad \text{for} \quad x, y \ll z. \tag{A.10}$$

$$R_J(x, y, z, p) = \tfrac{3}{2}\tfrac{1}{\sqrt{xyz}} \ln \tfrac{4xyz}{p\sigma^2} + 2R_J(x+\sigma, y+\sigma, z+\sigma, \sigma)$$
$$+ \mathcal{O}\Big(p \ln p\Big) \qquad \text{for} \quad p \ll x, y, z, \tag{A.11}$$

where $\sigma \equiv \sqrt{xy} + \sqrt{yz} + \sqrt{zx}$.

Note that the incomplete elliptic integrals could be represented by the symmetric forms as

$$F(\varphi \,|\, m) = R_F\Big(\tfrac{\cos^2 \varphi}{\sin^2 \varphi}, \ \tfrac{1}{\sin^2 \varphi} - 1, \ \tfrac{1}{\sin^2 \varphi}\Big), \tag{A.12}$$

$$\Pi(\nu\,;\,\varphi \,|\, m) = \sin\varphi \; R_F(\cos^2\varphi, \ 1 - m\sin^2\varphi, \ 1)$$
$$+ \frac{\nu}{3} \sin^3\varphi \; R_J(\cos^2\varphi, \ 1 - m\sin^2\varphi, \ 1, \ 1 - \nu\sin^2\varphi). \tag{A.13}$$

B   2d computation with AdS$_2$ matter contribution

We begin with the entanglement entropy the interval $\mathcal{I}_{RL}$ without any extra AdS$_2$ matter propagation. The two-point function with the twist operator insertion may be evaluated as

$$G_n^{RL} = \langle \Phi_n^+(P_R)\Phi_n^-(P_L)\rangle_{CFT} = \left[\frac{\sqrt{U_R^+ U_R^- U_L^+ U_L^-}}{(U_R^+ - U_L^+)(U_L^- - U_R^-)}\right]^{\Delta_n}. \tag{B.1}$$

In this expression, the numerator inside the bracket comes from the Weyl factor at each point in the Weyl transformation from the trivial flat metric $ds_f^2 = -dU^+dU^-$ to our metric in (8.3). In this appendix we shall omit the discussion involved with the issue of regularization and renormalization. Once we have two point function G_n, the corresponding entanglement entropy will be evaluated by

$$\hat{S} = -\lim_{n \to 1} \partial_n G_n \,. \tag{B.2}$$

Thus one finds that the entanglement entropy is given by $\hat{S}_{RL}$ in (8.21). Similarly, $\hat{S}_{Rr}$ can be evaluated using the two-point function

$$G_n^{Rr} = \langle \Phi_n^+(P_R)\Phi_n^-(P_r)\rangle_{CFT} = \left[\frac{\left(1 + U_r^+ U_r^-\right)\sqrt{-U_R^+ U_R^-}}{2(U_R^+ - U_r^+)(U_r^- - U_R^-)}\right]^{\Delta_n} \,. \tag{B.3}$$

This leads to

$$\hat{S}_{Rr} = \frac{c}{6}\left[\ln \frac{\cos(\tau - \tau_0) - \cos(\lambda - \lambda_0)}{\cos\lambda_0 \, \cos\lambda} + \ln 2\sinh\frac{2\pi}{\beta}x\right] \,. \tag{B.4}$$

By the same way, one may check that $\hat{S}_{Rr} = \hat{S}_{Ll}$, which may be understood from the left right symmetry of our configuration. For the AdS$_2$ matter contribution of the interval $\mathcal{I}_{rl}$, we use the two-point function of the boundary (interface) operator $\hat{O}_n$

$$G_n^{rl} = \langle O_n(P_r)O_n(P_l)\rangle_{CFT} = \left[\frac{\left(1 + U_r^+ U_r^-\right)\left(1 + U_l^+ U_l^-\right)}{4(U_r^+ - U_l^+)(U_l^- - U_r^-)}\right]^{\hat{\Delta}_n} \,. \tag{B.5}$$

This leads to

$$\hat{S}_{rl} = \frac{c\,\hat{q}}{3}\ln 2\tan\lambda_0 \,, \tag{B.6}$$

where we introduce $\hat{q}$ by

$$\hat{q} = \frac{6}{c}\partial_n\hat{\Delta}_n|_{n=1} \,. \tag{B.7}$$

We assume $0 < \hat{q} < 1$. Then the generalized entropy including the AdS$_2$ matter contribution is given by

$$\hat{S}_{gen} = \frac{c}{3}\left[\hat{q}\ln 2\tan\lambda_0 + \ln \frac{\cos(\tau - \tau_0) - \cos(\lambda - \lambda_0)}{\cos\lambda_0 \, \cos\lambda} + \ln 2\sinh\frac{2\pi}{\beta}x\right] \,. \tag{B.8}$$

Its extremization with respect to τ_0 is solved by $\tau_0 = \tau$. Then the extremization condition with respect to λ_0 becomes

$$\frac{1 + \cos(\lambda - \lambda_0)}{\sin(\lambda - \lambda_0)} = \hat{q}\big(\tan\lambda_0 + \cot\lambda_0\big) + \tan\lambda_0 \,. \tag{B.9}$$

44

Let us first consider the case where $|\tan\lambda|^2 = \xi \gg 1$ with ξ defined in (7.8). Then there are two solutions for the range $0 \le \lambda_0 < \frac{\pi}{2}$. One is

$$\tan\lambda_0^{(1)} = \frac{1-\hat{q}}{1+\hat{q}} \, |\tan\lambda| \left(1 + O(\xi^{-1})\right) , \tag{B.10}$$

which leads to the extremal value

$$\hat{S}_{(1)} = \frac{c}{3} \left[\hat{q} \ln \frac{2(1-\hat{q})\cosh\frac{2\pi}{\beta}t}{(1+\hat{q})\,\sinh\frac{2\pi}{\beta}x} + \ln \frac{4\sinh\frac{2\pi}{\beta}x}{1-\hat{q}^2} + O(\xi^{-1}) \right] . \tag{B.11}$$

The other solution is

$$\sin\lambda_0^{(2)} = \hat{q} + O(\xi^{-\frac{1}{2}}), \tag{B.12}$$

and the corresponding extremal value becomes

$$\hat{S}_{(2)} = \frac{c}{3} \left[\frac{\hat{q}}{2} \ln \frac{4\hat{q}^2}{1-\hat{q}^2} - \frac{1}{2} \ln \frac{1+\hat{q}}{1-\hat{q}} + \ln 2\cosh\frac{2\pi}{\beta}t + O(\xi^{-1}) \right] . \tag{B.13}$$

The minimum of (B.11), (B.13) and (8.21) gives us the true entanglement entropy. Note that in these solutions, the points $P_{r/l}$ lie behind-horizon region. Thus we find, for $\xi \gg 1$, $\hat{S} = \hat{S}_{(1)}$ which involves the behind-horizon AdS_2 matter contribution.

One may also consider $\xi \ll 1$. In this case, one finds no solution of the extremal condition (B.9) in the range $0 \le \lambda_0 < \frac{\pi}{2}$. Hence, for $\xi \ll 1$, $\hat{S} = \hat{S}_{RL}$ which does not involve any extra AdS_2 matter contribution.

References

[1] S. W. Hawking, "Particle Creation by Black Holes," Commun. Math. Phys. **43** (1975) 199 Erratum: [Commun. Math. Phys. **46** (1976) 206].

[2] S. W. Hawking, "Black hole explosions," Nature **248** (1974) 30.

[3] R. M. Wald, "On Particle Creation by Black Holes," Commun. Math. Phys. **45** (1975), 9-34

[4] G. 't Hooft, "The Scattering matrix approach for the quantum black hole: An Overview," Int. J. Mod. Phys. A **11** (1996), 4623-4688 [arXiv:gr-qc/9607022 [gr-qc]].

[5] S. D. Mathur, "The Fuzzball proposal for black holes: An Elementary review," Fortsch. Phys. **53** (2005) 793

[6] J. Polchinski, "The Black Hole Information Problem," arXiv:1609.04036 [hep-th].

[7] W. G. Unruh and R. M. Wald, "Information Loss," Rept. Prog. Phys. **80** (2017) no.9, 092002 [arXiv:1703.02140 [hep-th]].

[8] A. Ashtekar, "Black Hole evaporation: A Perspective from Loop Quantum Gravity," Universe **6** (2020) no.2, 21 [arXiv:2001.08833 [gr-qc]].

[9] J. Maldacena, "Black holes and quantum information," Nature Rev. Phys. **2** (2020) no.3, 123-125

[10] A. Almheiri, T. Hartman, J. Maldacena, E. Shaghoulian and A. Tajdini, "The entropy of Hawking radiation," [arXiv:2006.06872 [hep-th]].

[11] S. Hawking, "The Unpredictability of Quantum Gravity," Commun. Math. Phys. **87** (1982), 395-415

[12] T. Jacobson, "Introduction to quantum fields in curved space-time and the Hawking effect," [arXiv:gr-qc/0308048 [gr-qc]].

[13] T. Banks, L. Susskind and M. E. Peskin, "Difficulties for the Evolution of Pure States Into Mixed States," Nucl. Phys. B **244** (1984), 125-134

[14] A. Almheiri, D. Marolf, J. Polchinski and J. Sully, "Black Holes: Complementarity or Firewalls?," JHEP **1302** (2013) 062 [arXiv:1207.3123 [hep-th]].

[15] A. Almheiri, D. Marolf, J. Polchinski, D. Stanford and J. Sully, "An Apologia for Firewalls," JHEP **1309** (2013) 018 [arXiv:1304.6483 [hep-th]].

[16] J. Maldacena and L. Susskind, "Cool horizons for entangled black holes," Fortsch. Phys. **61** (2013) 781 [arXiv:1306.0533 [hep-th]].

[17] D. N. Page, "Information in black hole radiation," Phys. Rev. Lett. **71** (1993) 3743 [hep-th/9306083].

[18] R. Jackiw, "Lower Dimensional Gravity," Nucl. Phys. B **252** (1985) 343.

[19] C. Teitelboim, "Gravitation and Hamiltonian Structure in Two Space-Time Dimensions," Phys. Lett. **126B** (1983) 41.

[20] A. Almheiri, N. Engelhardt, D. Marolf and H. Maxfield, "The entropy of bulk quantum fields and the entanglement wedge of an evaporating black hole," JHEP **1912** (2019) 063 [arXiv:1905.08762 [hep-th]].

[21] G. Penington, "Entanglement Wedge Reconstruction and the Information Paradox," arXiv:1905.08255 [hep-th].

[22] A. Lewkowycz and J. Maldacena, "Generalized gravitational entropy," JHEP **08** (2013), 090 doi:10.1007/JHEP08(2013)090 [arXiv:1304.4926 [hep-th]].

[23] T. Faulkner, A. Lewkowycz and J. Maldacena, "Quantum corrections to holographic entanglement entropy," JHEP **11** (2013), 074 [arXiv:1307.2892 [hep-th]].

[24] N. Engelhardt and A. C. Wall, "Quantum Extremal Surfaces: Holographic Entanglement Entropy beyond the Classical Regime," JHEP **01** (2015), 073 doi:10.1007/JHEP01(2015)073 [arXiv:1408.3203 [hep-th]].

[25] A. Almheiri, R. Mahajan, J. Maldacena and Y. Zhao, "The Page curve of Hawking radiation from semiclassical geometry," JHEP **2003** (2020) 149 [arXiv:1908.10996 [hep-th]].

[26] S. Ryu and T. Takayanagi, "Holographic derivation of entanglement entropy from AdS/CFT," Phys. Rev. Lett. **96** (2006) 181602 [hep-th/0603001].

[27] V. E. Hubeny, M. Rangamani and T. Takayanagi, "A Covariant holographic entanglement entropy proposal," JHEP **07** (2007), 062 [arXiv:0705.0016 [hep-th]].

[28] D. Bak, M. Gutperle and S. Hirano, "A Dilatonic deformation of AdS(5) and its field theory dual," JHEP **05** (2003), 072 [arXiv:hep-th/0304129 [hep-th]].

[29] D. Bak, M. Gutperle and R. A. Janik, "Janus Black Holes," JHEP **1110** (2011) 056 [arXiv:1109.2736 [hep-th]].

[30] P. Calabrese and J. L. Cardy, "Entanglement entropy and quantum field theory," J. Stat. Mech. **0406** (2004), P06002 [arXiv:hep-th/0405152 [hep-th]].

[31] M. Rozali, J. Sully, M. Van Raamsdonk, C. Waddell and D. Wakeham, "Information radiation in BCFT models of black holes," JHEP **05** (2020), 004 [arXiv:1910.12836 [hep-th]].

[32] V. Balasubramanian, A. Kar, O. Parrikar, G. Srosi and T. Ugajin, "Geometric secret sharing in a model of Hawking radiation," [arXiv:2003.05448 [hep-th]].

[33] J. Sully, M. Van Raamsdonk and D. Wakeham, "BCFT entanglement entropy at large central charge and the black hole interior," [arXiv:2004.13088 [hep-th]].

[34] H. Z. Chen, R. C. Myers, D. Neuenfeld, I. A. Reyes and J. Sandor, "Quantum Extremal Islands Made Easy, Part I: Entanglement on the Brane," arXiv:2006.04851 [hep-th].

[35] D. Bak, M. Gutperle and S. Hirano, "Three dimensional Janus and time-dependent black holes," JHEP **0702** (2007) 068 [hep-th/0701108].

[36] M. Banados, C. Teitelboim and J. Zanelli, "The Black hole in three-dimensional space-time," Phys. Rev. Lett. **69** (1992), 1849-1851 [arXiv:hep-th/9204099 [hep-th]].

[37] T. Hartman and J. Maldacena, "Time Evolution of Entanglement Entropy from Black Hole Interiors," JHEP **1305** (2013) 014 [arXiv:1303.1080 [hep-th]].

[38] I. Affleck and A. W. Ludwig, "Universal noninteger 'ground state degeneracy' in critical quantum systems," Phys. Rev. Lett. **67**, 161-164 (1991)

[39] J. M. Maldacena, "Eternal black holes in anti-de Sitter," JHEP **0304** (2003) 021 [hep-th/0106112].

[40] A. Almheiri, R. Mahajan and J. Maldacena, "Islands outside the horizon," arXiv:1910.11077 [hep-th].

[41] A. Almheiri, T. Hartman, J. Maldacena, E. Shaghoulian and A. Tajdini, "Replica Wormholes and the Entropy of Hawking Radiation," JHEP **2005** (2020) 013 [arXiv:1911.12333 [hep-th]].

[42] G. Penington, S. H. Shenker, D. Stanford and Z. Yang, "Replica wormholes and the black hole interior," [arXiv:1911.11977 [hep-th]].

[43] H. Liu and S. Vardhan, "A dynamical mechanism for the Page curve from quantum chaos," arXiv:2002.05734 [hep-th].

[44] P. Caputa, J. Simn, A. tikonas, T. Takayanagi and K. Watanabe, "Scrambling time from local perturbations of the eternal BTZ black hole," JHEP **1508** (2015) 011 [arXiv:1503.08161 [hep-th]].

[45] T. Faulkner, H. Liu and M. Rangamani, "Integrating out geometry: Holographic Wilsonian RG and the membrane paradigm," JHEP **1108** (2011) 051 [arXiv:1010.4036 [hep-th]].

[46] M. Chiodaroli, J. Estes and Y. Korovin, "Holographic two-point functions for Janus interfaces in the $D1/D5$ CFT," JHEP **1704** (2017) 145 [arXiv:1612.08916 [hep-th]].

[47] D. Maz, L. Rastelli and X. Zhou, "An analytic approach to BCFT$_d$," JHEP **1912** (2019) 004 [arXiv:1812.09314 [hep-th]].

[48] M. Alishahiha, A. Faraji Astaneh and A. Naseh, "Island in the Presence of Higher Derivative Terms," [arXiv:2005.08715 [hep-th]].

[49] C. Krishnan, V. Patil and J. Pereira, "Page Curve and the Information Paradox in Flat Space," [arXiv:2005.02993 [hep-th]].

[50] Frank W. Olver, Daniel W. Lozier, Ronald F. Boisvert, Charles W. Clark, "NIST Handbook of Mathematical Functions," Cambridge University Press, New York, NY, 2010.